JOURNAL OF GEOPHYSICAL RESEARCH, VOL. 98, NO. D6, PAGES 10,777–10,797, JUNE 20, 1993

THE HALOGEN OCCULTATION EXPERIMENT

James M. Russell III,[1] Larry L. Gordley,[2] Jae H. Park,[1] S. Roland Drayson,[3]
W. Donald Hesketh,[4] Ralph J. Cicerone,[5] Adrian F. Tuck,[6]
John E. Frederick,[7] John E. Harries,[8] and Paul J. Crutzen[9]

Abstract. The Halogen Occultation Experiment (HALOE) was launched on the Upper Atmosphere Research Satellite (UARS) spacecraft September 12, 1991, and after a period of outgassing, it began science observations October 11. The experiment uses solar occultation to measure vertical profiles of O_3, HCl, HF, CH_4, H_2O, NO, NO_2, aerosol extinction, and temperature versus pressure with an instantaneous vertical field of view of 1.6 km at the Earth limb. Latitudinal coverage is from 80°S to 80°N over the course of 1 year and includes extensive observations of the Antarctic region during spring. The altitude range of the measurements extends from about 15 km to ≈ 60-130 km, depending on channel. Experiment operations have been essentially flawless, and all performance criteria either meet or exceed specifications. Internal data consistency checks, comparisons with correlative measurements, and qualitative comparisons with 1985 atmospheric trace molecule spectroscopy (ATMOS) results are in good agreement. Examples of pressure versus latitude cross sections and a global orthographic projection for the September 21 to October 15, 1992, period show the utility of CH_4, HF, and H_2O as tracers, the occurrence of dehydration in the Antarctic lower stratosphere, the presence of the water vapor hygropause in the tropics, evidence of Antarctic air in the tropics, the influence of Hadley tropical upwelling, and the first global distribution of HCl, HF, and NO throughout the stratosphere. Nitric oxide measurements extend through the lower thermosphere.

1. Experiment Introduction and Objectives

Considerable attention has been focused on the middle atmosphere (10 km to 100 km) in recent years because of concerns that anthropogenic activity can alter the natural composition of the region and lead to ozone depletion. These concerns have now been realized with the discovery by Farman et al. [1985] of a deep total ozone minimum over Halley Bay (75.5°S, 26.8°W) that has occurred annually since the mid-1970s in September and October. This Antarctic ozone "hole" which is characterized by 50% or more decreases in column ozone has now been extensively studied using satellite, aircraft, and ground-based instruments. In addition, further analyses of satellite and ground-based Dobson data have shown northern hemisphere (30°N to 64°N) ozone declines over the period 1969 to 1988 of 3 to 5% during winter months. These changes cannot be explained by known natural processes [World Meteorological Organization (WMO), 1990]. More recently, an update to the WMO study shows that the summertime ozone column in the northern hemisphere temperate zones also has decreased by about 3% in the 1980s. A succinct summary and discussion of theories describing the Antarctic ozone hole phenomenon has been presented by Solomon [1990]. Evidence shows that enhanced chlorine levels in the presence of aerosols and particles is leading to reactions that cause Antarctic ozone depletion. Changes occurring in the mid-latitudes, however, especially in the summertime, are not completely understood. Since ozone has such profound effects on human health, crop growth, and the climate, it is vital that a thorough understanding of those factors affecting its distribution be developed so that appropriate corrective actions or other planning steps can be taken.

The Halogen Occultation Experiment (HALOE) was conceived to provide critical data for study of the ozone distribution and those processes which affect ozone levels. The experiment uses the principle of satellite solar occultation to sound the stratosphere, mesosphere, and lower thermosphere. Using this technique, absorption of solar energy in selected spectral bands is used to infer vertical profiles of temperature, pressure, and mixing ratios of key gases involved in the ozone chemistry. The HALOE instrument includes both broadband and gas filter channels covering selected portions of the spectral range from 2.45 μm to 10.04 μm. The experiment was launched onboard the Upper Atmosphere Research Satellite (UARS) spacecraft by the Space Shuttle Discovery at 19:11:04 eastern daylight time on September 12, 1991. A science team (authors of this paper) was formed to guide the experiment development, assist in flight data validation, and carry out scientific investigations.

The HALOE experiment was first proposed in 1975 shortly after the initial paper was published by Molina and Rowland [1974] discussing the possible effects of chlorofluorocarbons (CFCs) on atmospheric ozone. The essentials of the gas filter technique used in the occultation mode have been described by Russell et al. [1977]. The technique builds on the same general method employed by the Monitoring of Air Pollution by Satellite (MAPS) experiment [Reichle et al., 1990]. The MAPS instrument makes gas filter nadir-viewing observations

[1]Atmospheric Sciences Division, NASA Langley Research Center, Hampton, Virginia.
[2]GATS, Incorporated, Hampton, Virginia.
[3]University of Michigan, Ann Arbor, Michigan.
[4]SpaceTec Ventures, Incorporated, Hampton, Virginia.
[5]University of California/Irvine, Irvine, California.
[6]NOAA Aeronomy Laboratory, Boulder, Colorado.
[7]University of Chicago, Chicago, Illinois.
[8]Rutherford Appleton Laboratory, Oxfordshire, England.
[9]Max Planck Institute for Chemistry, Mainz, Germany.

Paper number 93JD00799.
0148-0227/93/93JD-00799$05.00

of upwelling energy at 4.6 μm, which are then mathematically inverted to infer the concentrations of tropospheric carbon monoxide. The experiment has been successfully flown and operated on two Space Shuttle missions. The sensitivity of the HALOE gas filter measurement is about 1 order of magnitude better than that achieved with the MAPS instrument. This improvement is necessary in order to sound the tenuous gases of the middle atmosphere. The HALOE instrument was jointly designed by TRW, Incorporated, and the Langley Research Center. Fabrication, testing, and calibration was performed at the Langley Research Center.

The overall scientific goal of HALOE is to provide global scale data on temperature, ozone, odd chlorine (ClO_y), odd nitrogen (NO_y), and odd hydrogen (HO_y) compounds needed to study the chemistry and dynamics processes of the middle atmosphere. A primary objective is to analyze the data to provide improved understanding of the magnitude, time history, geographic variations, and causes of ozone change. The list of gases being observed by HALOE includes ozone (O_3) itself, the chlorine reservoir hydrogen chloride (HCl), catalysts in O_3 destruction by odd nitrogen-nitric oxide and nitrogen dioxide (NO and NO_2, respectively), source gases for odd hydrogen-methane and water vapor (CH_4 and H_2O), and the fluorine reservoir hydrogen fluoride (HF). Together, these observations form a minimum but adequate set which can be used to derive, under appropriate conditions, the unmeasured concentrations of several other gases needed to test understanding of the chemistry (see Figure 1). In this regard, HALOE O_3, H_2O, and CH_4 measurements, for example, can be used to derive OH levels. In turn, these parameters can be used to derive atomic chlorine and, from that, ClO through reactions with O_3. Chlorine monoxide can be used with NO_2 observations to derive chlorine nitrate ($ClONO_2$). Since ClO and $ClONO_2$ are being observed by other UARS experiments (MLS and CLAES, respectively) at a different time of day, a stringent test of photochemical theory can be carried out using a two-dimensional model and comparing theory and observations. Such a test can also be aided by balloon or ground-based correlative measurements.

A second key objective of HALOE is to study the impact of the CFCs on ozone using the HF and HCl data. Since the primary man-made chlorine sources (i.e., the CFCs) contain both chlorine and fluorine in the molecule, while the natural sources (e.g., CH_3Cl) contain only chlorine, HF (a postdissociation product of the CFCs) becomes an indicator of anthropogenic chlorine input to the middle atmosphere. Hydrogen chloride, on the other hand, is an indicator of total chlorine input from both natural and man-made sources. The relative importance of these two sources of stratospheric chlorine can be inferred by studying changes in HCl and HF with time. The ratio of HCl/HF also is a useful indicator of perturbed chemistry in the presence of stratospheric aerosols. According to theory [e.g., Solomon, 1990], and as observations suggest [e.g., Mankin et al., 1991], this ratio is significantly reduced when aerosols are present at low temperatures due to HCl-destroying reactions that do not normally occur in the gas phase.

This paper describes the HALOE experiment, the results of ground testing, and initial performance in orbit. Section 2 describes the measurement approach in more detail and discusses measurement requirements. Section 3 describes the geographic coverage of the HALOE measurements. Sections 4 and 5 discuss the instrument and performance, data processing, and the inversion approach. Section 6 describes data validation studies, and section 7 presents initial measurement results.

2. Measurement Approach and Requirements

The objectives of the HALOE experiment are met by measuring the absorption of solar energy due to stratospheric gases during spacecraft sunrise and sunset. The experiment geometry is illustrated in Figure 2 [see e.g., Russell, 1980]. Absorption is measured as a function of tangent height pressure defined as the pressure at the altitude (H_o) of the closest approach of a ray path to the Earth surface. A vertical scan of the atmosphere is obtained by tracking the Sun position during occultation. Measurements made in the Earth limb absorption mode have the advantage of higher sensitivity than is possible when viewing in the nadir since the limb path contains from 30 to 60 times more absorber. High vertical resolution can be achieved because of the limb geometry and the exponential decrease of density with altitude. This results in most of the absorption occurring at or near the tangent point. Another advantage of solar occultation is that a relative measurement is made. Each gas mixing ratio vertical profile is determined by ratioing the solar energy reduced by atmospheric attenuation with the unattenuated solar energy measured outside the atmosphere. This makes the instrument

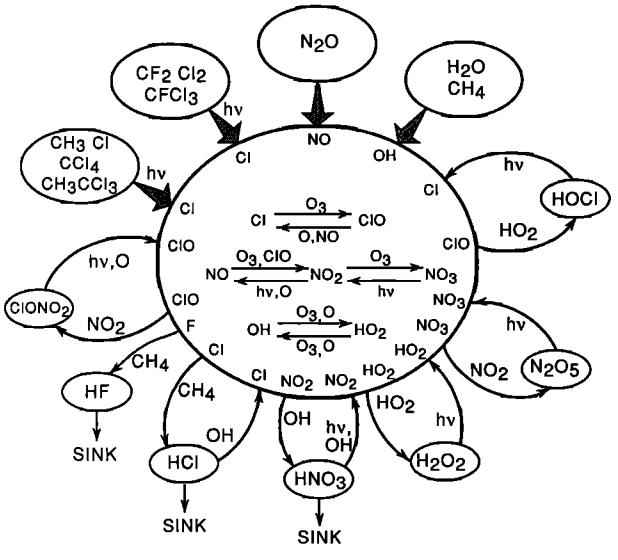

Fig. 1. Simplified middle atmosphere chemistry.

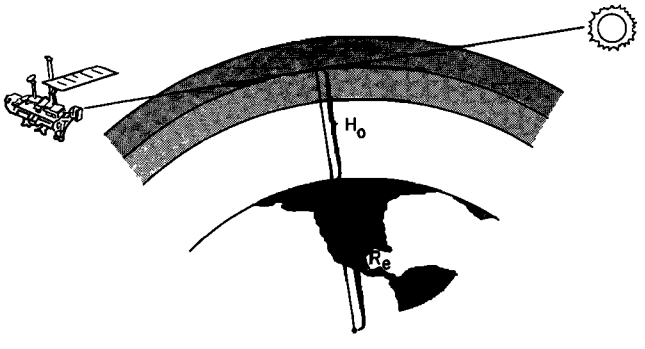

Fig. 2. Solar occultation experiment geometry.

virtually self-calibrating and especially useful in the study of long-term trends since errors due to unaccounted for drifts are greatly reduced. Some disadvantages of the occultation approach are that measurements are made only at the sunrise and sunset times, geographic coverage is constrained by the Earth-Sun geometry, and the measurement sampling rate is limited to 15 sunrises and 15 sunsets each day.

2.1. Basic Equations

A schematic of the broadband HALOE measurement approach is shown in Figure 3. The measured voltage V for a broad spectral band of width $\Delta\nu$, where ν is wavenumber, can be expressed by

$$V_{\Delta\nu} = CA\tau \int_{\Delta\nu} N_s(\nu)\, \Gamma(\nu)\, \tau_a(\nu, q, P, T)\, d\nu \qquad (1)$$

where C is a responsivity factor, A is instrument aperture area, τ is an optical and electronic efficiency factor, $N_S(\nu)$ is the solar intensity at wavenumber ν, $\Gamma(\nu)$ is the spectral response function of the instrument, τ_a is the transmission of the atmosphere, q is gas mixing ratio, and P and T are the atmospheric pressure and temperature, respectively. When the

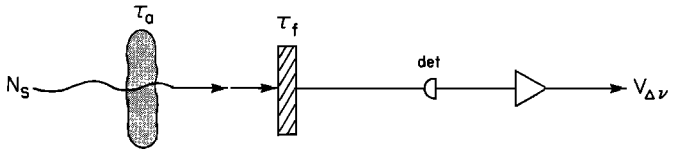

Fig. 3. The Halogen Occultation Experiment (HALOE) broadband radiometer measurement concept.

Sun is viewed exoatmospherically, $\tau_a = 1.0$ and $V_{\Delta\nu} = V_o$, the unattenuated signal. The atmospheric transmission averaged over the spectral band is determined by ratioing the signal $V_{\Delta\nu}$ at any altitude (or pressure level) with V_o. Since transmission is dependent on temperature, pressure, and mixing ratio, measurements are processed first for a spectral band where the gas mixing ratio is known (2.8 μm CO_2 band in this case) in order to infer the temperature versus pressure vertical profile. Next, transmission measurements made in other spectral bands (e.g., NO_2, H_2O, or O_3) are used to infer the unknown mixing ratios. Two approaches are used in HALOE processing to obtain a vertical temperature versus pressure profile. Initially, the measured CO_2 transmittances are compared with calculated transmittances obtained by assuming a constant CO_2 mixing ratio profile and using National Meteorological Center (NMC) temperature versus pressure data. The differences in these transmittances are used to register the vertical HALOE signal profile in the NMC pressure space. Next, the CO_2 transmissions are used to retrieve temperature versus pressure which extends to a higher altitude than the NMC product. Pressure registration can also be attempted using the vertical solar extent measured by HALOE as a function of altitude and the calculated extent obtained using the NMC profile. The presence of Mount Pinatubo aerosol layers greatly complicates these approaches, and in the early stages of the mission, only the CO_2 transmittances measured at and above about 25-30 km in altitude are being used for pressure registration and temperature versus pressure retrieval. NMC values are used below about 30 km.

Equation (1) expresses the measured voltage $V_{\Delta\nu}$ resulting from a weighted average over the spectral band pass $\Delta\nu$ and for a spectral response function $\Gamma(\nu)$. The real HALOE instrument signal is also weighted by spatial averaging due to the instantaneous vertical field-of-view (IFOV) function of the instrument. When this factor is included, the measured voltage V is given by

$$V = CA\tau \iiint_{\theta\,\phi\,\nu} N_s(\nu,\theta,\phi)\Gamma(\nu)\, \gamma(\theta,\phi)\tau_a(\nu,q,P,T,\theta,\phi)\, d\nu d\theta d\phi \qquad (2)$$

where θ and ϕ represent azimuth and elevation angle, $\gamma(\theta, \phi)$ is the instrument spatial response function, and the angular dependencies are now reflected in the arguments of the solar intensity and transmission functions. Complete rigor in forward calculations using the source function $N_S(\nu, \theta, \phi)$ would require averaging over the HALOE IFOV in both the azimuth and the elevation directions in order to match the measured signals. Instead of this approach, the effect is handled in data processing by retrieving a parameterized single-dimensional (elevation direction) limb-darkening curve which matches the two dimensionally averaged HALOE signal obtained from spatial scans of the solar disk. Simulations have shown that this approach leads to negligibly small errors.

The HALOE instrument tracks the Sun with the infrared telescope locked at a point below the top solar edge. As an event progresses (e.g., sunset), the circular solar image becomes elliptical with the lower edge of the Sun becoming flatter at low tangent altitudes due to refraction effects. The apparent Sun extent decreases, and the center of the telescope IFOV moves, in effect, toward the center of the Sun and, ultimately, past the center. At the same time, the IFOV covers an increasingly larger area of the solar disk. These effects must be rigorously considered in the forward calculations used for inverting measurements to obtain temperature and mixing ratio. Accurate knowledge of the IFOV-averaged solar limb-darkening curve is required for every measurement point in order to hold errors in retrieved parameters to small values.

The measurement approach described thus far leads to definition of several requirements. Simulations and experience in orbit show that the lock point should be from 4 to 8 arc min down from the top edge in order to reduce solar pointer/tracker induced noise on the infrared signals and to further penetrate the Mount Pinatubo aerosol layer before loss of Sun tracker signal occurs due to aerosol attenuation. The pointing knowledge required to reduce measured transmission errors to $\approx \leq 0.1\%$ is ± 12 arc sec in elevation and ± 15 arc sec in azimuth (1σ). The IFOV is specified to be narrow enough to measure a feature ≤ 2 km in vertical extent with IFOV "skirts" sharp enough to allow measurements to be made within 2 km of a tropospheric cloud feature and have only a small effect (< 3%) on the measured signal. The spectral filter functions for each channel need to be sufficiently narrow to isolate the spectral band of interest while rejecting most of the absorption lines from interfering gases. This requires bandwidths as narrow as 26 cm^{-1} in some instances. Measured transmittance noise levels must be of the order of ≤ 0.1% in order to obtain good accuracy in the lower and upper

stratosphere where either saturated absorption or very little absorption, respectively, occurs.

The use of the broadband radiometer approach is possible when a dominant absorbing gas can be spectrally isolated. This is not always possible, and more sophisticated instrument techniques must be used. An example of this is the HCl measurement. The strongest HCl absorption lines occur at 3.4 μm, which is in the middle of the strongest CH_4 band in nature. Measurement of HCl is made more difficult by the approximately 1000 times greater CH_4 concentration. The nature of the problem is shown by the calculated limb absorption spectrum at the 30-km tangent height in the HALOE HCl band (Figure 4). As can be seen, CH_4 is the dominant absorber, and the effect of HCl on the broadband absorption is very small. Under these circumstances, a high spectral resolution measurement is required. The HALOE measurement approach used for HCl, HF, CH_4, and NO is gas filter radiometry.

The HALOE gas filter instrument concept is illustrated schematically in Figure 5. Solar energy N_S passing through the HALOE filter with transmission τ_f is split into two paths; one includes a gas cell containing the gas of interest (e.g., HCl in Figure 5) with transmission τ_g, and the second is a vacuum path with transmission τ_v. After detection by detectors D_1 and D_2, the signals are sent to a differencing amplifier where voltage ΔV is developed. The instrument is balanced to a zero ΔV value (to within the system noise) using the electronic gain adjustment G in the gas path when HALOE views the Sun outside the atmosphere ($\tau_a = 1.0$). When the target (e.g., HCl) gas is encountered in the atmosphere during sunrise or sunset, an atmospheric transmission τ_a arises which causes ΔV and V to change. These changes can then be related to the tangent point mixing ratio. The required sensitivity in order to measure tenuous gases like HCl and HF is that the instrument be capable of measuring radiance differences of 2 parts in 10^5. This value was determined based on retrievals using simulated noisy signals derived from the expected vertical profiles of HCl and HF.

The gas filter channel modulation signal, M, can be formulated with considerable algebra into a succinct function; we state only the result here.

$$M = \frac{\Delta V}{V} = (\bar{G} - 1)\left[\frac{\bar{\tau}_w - \bar{\tau}_N}{\bar{\tau}_w}\right] \tag{3}$$

where

$$\bar{\tau}_w = \frac{\int_{\nu_1}^{\nu_2} N_S \tau_a F_W \, d\nu}{\int_{\nu_1}^{\nu_2} N_S F_W \, d\nu} \tag{4}$$

$$\bar{\tau}_N = \frac{\int_{\nu_1}^{\nu_2} N_S \tau_a F_N \, d\nu}{\int_{\nu_1}^{\nu_2} N_S F_N \, d\nu} \tag{5}$$

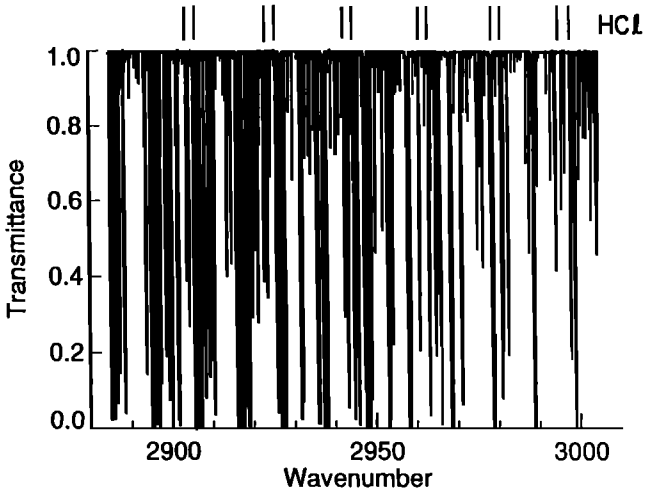

Fig. 4. Calculated 30-km absorption spectrum in the HALOE HCl channel. Positions of the HCl lines are shown by the tic marks at the top.

F_N is the narrow-band spectral function, and F_W is the wideband spectral function. Note that the gain adjust value $\bar{G}$ is equivalent to the reciprocal of the mean gas cell transmission τ_g. Thus the modulation signal M is made up of two terms; one is weighted by a narrow-band spectral function F_N and the other by a wideband function F_W. The wideband function is simply the instrument spectral response for the vacuum path given by

$$F_W = \tau_{fw} \tau_c \tau_v \tag{6}$$

where τ_{fw} is the broadband interference filter response, τ_c is the transmission of common optics before the beamsplitter is encountered, and τ_v is the transmission of the vacuum path optics. The transmissions τ_c and τ_v are shown schematically in Figure 5 as two optical elements although, in reality, they result from reflections and transmissions of all the optical elements in the optical train from the telescope to the detector. The narrow-band spectral function is defined by the expression

$$F_N = \tau_{fw} \tau_c \left[\tau_v - \frac{\tau_g \tau_1}{(\overline{\tau_1/\tau_2})}\right] \tag{7}$$

where

$$\left(\overline{\frac{\tau_1}{\tau_v}}\right) = \frac{\int_{\nu_1}^{\nu_2} N_S \tau_{fw} \tau_c \tau_1 \, d\nu}{\int_{\nu_1}^{\nu_2} N_S \tau_{fw} \tau_c \tau_v \, d\nu} \tag{8}$$

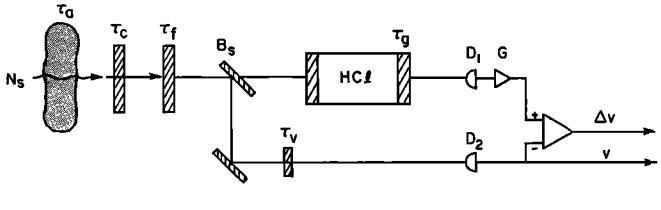

Fig. 5. The HALOE gas filter radiometer concept.

τ_g is transmission of gas in the gas cell and τ_1 is the transmission of the optics unique to the gas path. The τ_1 is primarily the product of transmission of the gas cell windows and the transmission of the focusing lenses just before the detectors. The narrow-band spectral function can have negative values, but the integral of F_N over the band pass is equal to the integrated absorption over the gas cell absorption lines. The narrow-band and wideband functions for HCl, as an example, are shown in Figures 6 and 7. Note that the narrow-band function has negative values between the HCl absorption lines in some regions. An ideal F_N would have zero value between absorption lines in order to provide the best rejection of interfering gas effects. The nonzero values occurred in the HCl channel because of slight differences in the gas and vacuum path detector spectral responses. Nearly ideal functions were achieved for the HF, CH_4, and NO channels. The quantity N_S, as before, represents the solar irradiance, and ν is wavenumber. For simplicity, the wavenumber and angle arguments have been dropped from the notation.

The wideband term, $\bar{\tau}_W$, which contains most of the interfering gas signal effects can be either modeled or measured directly by the vacuum path voltage $\underline{V}$. Therefore using equation (3) the narrow-band term, τ_N, can be formulated as a function of only measured parameters. The narrow-band signal also contains a residual interfering gas signal due to absorption overlap from the wings of adjacent lines of interfering gases.

The high HALOE sensitivity [noise equivalent modulation (NEM) is equal to 2×10^{-5}] means that the instrument is also sensitive to error effects due, for example, to slight changes in optical alignment caused by thermal changes in the instrument or, as another example, small fixed misalignments in the field of views of the two detectors on the horizon. These and other effects have been well characterized as explained in section 4 of this paper. Adjustments to the modulation signal to correct for thermal alignment changes or changes in detector responsivity during an occultation event can be made in two ways. One approach is to use an on-board reference blackbody (1100 K) source signal. The reference blackbody signal, which should be completely stable during an event, is a proxy for the solar signal. If the integrated intensity on one detector changes relative to the other detector due to optical

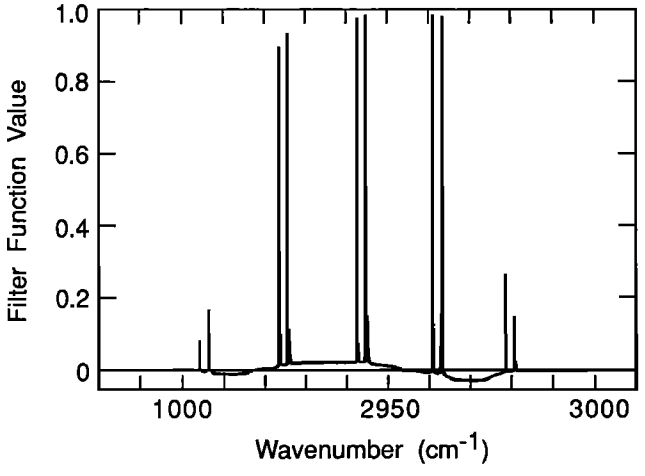

Fig. 6. HALOE HCl channel narrow-band spectral function F_N.

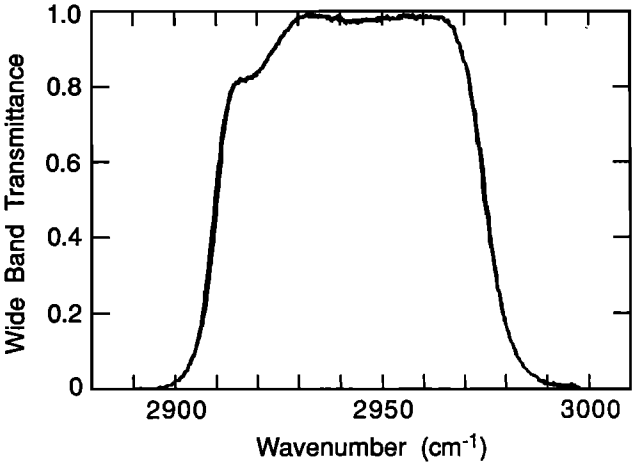

Fig. 7. HALOE wideband spectral function F_W.

change (e.g., beam misalignments) arising from thermal stresses, for example, then changes in the ΔR blackbody reference signal (analogous to ΔV) can be used to adjust the ΔV. This signal is derived by chopping the proxy solar energy at a different rate than the incoming solar signal. A second approach is to empirically determine the drift rate in ΔV using the exoatmospheric part of the occultation and assume a linear correction with altitude. Experience in orbit shows that this latter method works very well. Therefore the use of ΔR is only a backup approach.

The gas filter method leads to additional measurement requirements not applicable to broadband radiometry. The noise specification of 2 parts in 10^5 has been noted. Errors in the electronics gain relationship between the ΔV and the V signals creates a direct one-for-one error in the modulation signal. Therefore these relationships must be accurately known to the few percent level. These gains can be directly measured to less than 0.5% using orbital data. The pressure and mixing ratio knowledge required for the gas cells varies by channel but generally is of the order of 3%. This fixes the gas filter function. Once the gas filter has been characterized, the absolute pressure and mixing ratios are not important, only that the spectral filter defined by the gas is stable during the mission. Temperature effects on gas absorption have been considered, and thermistors are included in the instrument to measure gas cell temperatures, although this is a small effect. The ability to balance the ΔV signal inorbit to within several NEMs is required to keep signals from saturating prematurely due to component drifts that create imbalances between the gas and the vacuum path signals. The balance can also change due to changing solar intensity on the detectors. This occurs primarily because of detector response nonlinearity effects. This effect must be limited to 1 to 50 NEMs, depending on channel. The drift in signal during an event due to thermal effects must be less than 1 to 10 NEMs, depending on channel, so that sufficiently accurate corrections can be made, if required. Another factor that is important to consider is field-of-view mismatch. This arises because of the inability to perfectly match the gas and vacuum path detector effective IFOVs on the limb. Consequently, when one detector is displaced from the other in the vertical (altitude) direction and a transmission slope is encountered, a signal develops which has little to do with the target gas. The goal is that the effective mismatch be ≤ 0.1 arc sec. Both of these quantities (drift and

IFOV mismatch) are actually smaller in orbit than required. Cross talk between the ΔV and the ΔR signals (an electronic effect) needs to be less than 10 to 50 NEMs, depending on channel, in order to be able to make a useful correction for drift effects which occur during an occultation event. The cross-talk values can be measured in orbit to within a few percent and errors in these quantities are considerably less than required.

The gas filter radiometer measurement approach can be particularly effective when sounding in the presence of heavy aerosol loading. If we assume to first order that the aerosol transmittance over a narrow spectral band (44 to 110 cm^{-1} for the gas filter channels) is spectrally flat, then equation (3) shows that the measured modulation will be unaltered when aerosols are encountered since the spectrally constant aerosol transmittance appears in every term. Our signal simulations using actual aerosol spectral slopes across the gas filter band show that spectral effects due to the aerosol are negligible. Another important factor which can cause signal changes when the aerosol layer is encountered on the limb is field-of-view mismatch. This has been well characterized in the laboratory and verified in orbit for all gas filter channels. Also, a correction function to remove the mismatch has been developed. Under these assumptions then, the effect of aerosols on a gas filter measurement should be small. Our experience in orbit shows that only HCl and HF are affected by the mismatch effect, and it appears to cause no more than ≈ 0.3 parts per billion by volume (ppbv) changes in retrieved mixing ratios. Sometimes, early in the mission the aerosol extinction was so large at low altitudes that the signal was lost or extremely small and a measurement was not possible. As the Mount Pinatubo aerosol layer has subsided with time, however, this has now become less of a problem.

3. Geographic Coverage

The UARS was launched into a 585 km, 57° inclined, precessing orbit with an orbit repeat time over a geographic point about every 4-1/2 days. HALOE, in this orbit, provides coverage from about 80°S to 80°N over the course of the year (Figure 8). The launch time of day also affects the latitude coverage for any particular time of year. The effect of these and other parameters on an occultation experiment coverage has been described by Harrison and Gibson [1981]. We note in Figure 8 that HALOE observes at the most extreme southern latitudes during mid-September through early October, which includes the time of maximum ozone loss rate as the Antarctic ozone hole develops and recovers. During this time, an abundance of samples are taken in the Antarctic as shown by the polar stereographic projection of HALOE samples (Figure 9) for a 21-day period starting September 20, 1992. Note also that at certain times of the year (end of December and June) no occultations occur for a number of days since, at that time, the Earth-Sun line is normal or nearly normal to the orbit plane.

A total of 30 occultations occur each day usually with 15 sunrises and 15 sunsets happening in opposite hemispheres. This provides 900 events a month or approximately 10,800 occultations in a year. The combination of Earth rotation, orbit motion, and occultation sampling gives a measurement pattern with points always spiraling around the globe up or down in latitude with the greatest number of samples occurring at the

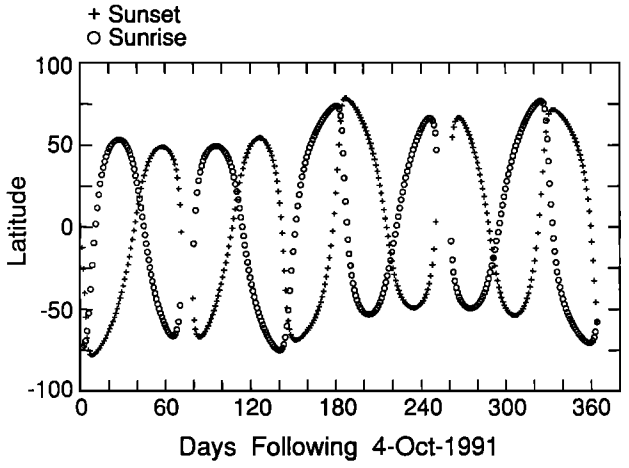

Fig. 8. HALOE latitude versus time coverage for 1 year.

extreme latitude positions. All nine HALOE parameters are measured for every occultation event. As an example, latitude versus longitude coverage for the month of November 1991 is shown in Figure 10. During this month, soundings were made from 60°S to 53°N.

4. Instrument Description and Performance

4.1. Instrument Description

General description of the main components of the HALOE instrument (Figure 11) include the sensor assembly containing the infrared telescope and optical mainframe, the biaxial gimbal assembly to provide solar tracking in the azimuth and elevation directions, the Sun sensor assembly, the on-gimbal electronics assembly (GEA), and the platform electronics assembly (PEA). Figure 11 shows the telescope dust cover door in place, radiator surfaces for cooling the optical mainframe and GEA, and the spacecraft adapter mounting plate. Thermal control of HALOE is maintained by (1) multilayer insulation which covers the entire instrument, (2) the radiator surfaces shown, and (3) strip heaters located on the primary and secondary mirrors of the telescope, on the Sun sensor assembly, on the gas channel and mainframe radiator surfaces, and on the spacecraft adapter. The instrument flies in an inverted position from that shown in the figure. The launch configuration included pyrotechnic actuators to cage the gimbals and hold the telescope door closed. The gimbals were released four days after launch on September 16, and the telescope door was opened October 2. The delay in door opening was to allow time for spacecraft outgassing to occur. Science data collection viewing the Sun was delayed another nine days until October 11 to allow more time for the instrument to outgas through the telescope. A special concern exists when an instrument is solar viewing since the Sun energy can polymerize foreign material, thereby fixing the contamination on the mirror surface and permanently changing the instrument spectral response in an unknown way. Hydrocarbons have absorption features that coincide with the spectral positions of the HCl and CH_4 channels. Hence, great caution was used in activating HALOE, and similar considerations have been used in operating the instrument inorbit so that contamination effects will be minimized.

The GEA contains the power conditioning, thermal control, data acquisition, and data handling electronics which require

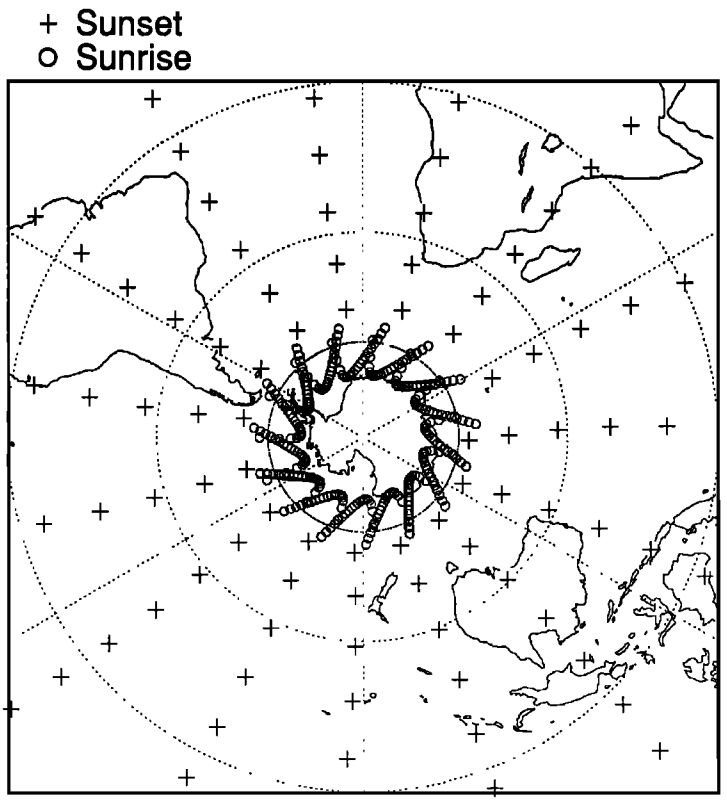

Fig. 9. HALOE Antarctic coverage for 21 days starting September 20, 1992.

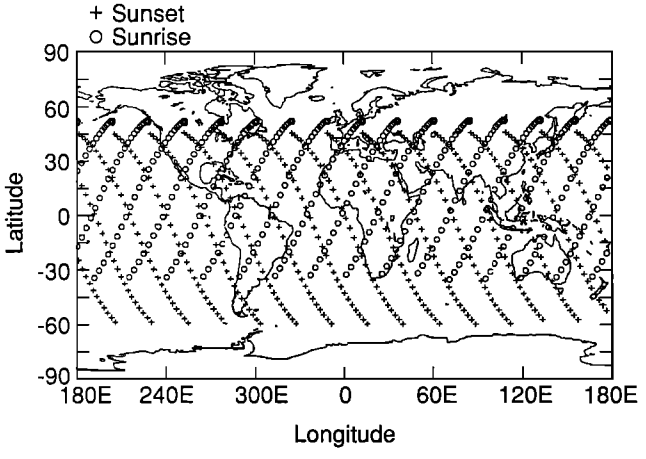

Fig. 10. HALOE latitude versus longitude coverage for the month of November 1991.

close proximity to both the Sun pointer/tracker and the sensor subsystems mounted on the optical mainframe. This allowed preamplification of detector signals at an early stage in the electronics, thereby allowing low noise to be achieved. The PEA contains the instrument low- noise power supply, motor drive, timing, control electronics, and spacecraft interface. These two assemblies distribute power; command, operate, and control the complete instrument; and collect, process, and format both science and engineering data for transmission to the ground.

The instrument size is approximately 93 cm (from spacecraft adapter to the frame radiator) by 62 cm (from the elevation drive edge to the telescope barrel edge), by 81 cm (from the front of the telescope to the GEA). The PEA dimensions are 23.5 x 24.3 x 22.1 cm, and the total mass of the sensor assembly plus PEA is 101 kg. The power consumption is 120 W, and the data rate is 4096 bits per second.

Instrument optics. The HALOE telescope collects solar energy using a diffraction-limited design Cassegrain telescope with a 16-cm-diameter primary mirror having a 96-cm focal length (*f*/6.6 beam). The overall optical schematic is shown in Figure 12. The optical material for the telescope mirrors is zerodur, and all optical lenses in the instrument are germanium. The telescope was manufactured as a module and rigidly mounted to a stiff aluminum honeycomb structure optical mainframe. Mainframe rigidity is critical in a gas filter instrument. After passing through the telescope, the energy

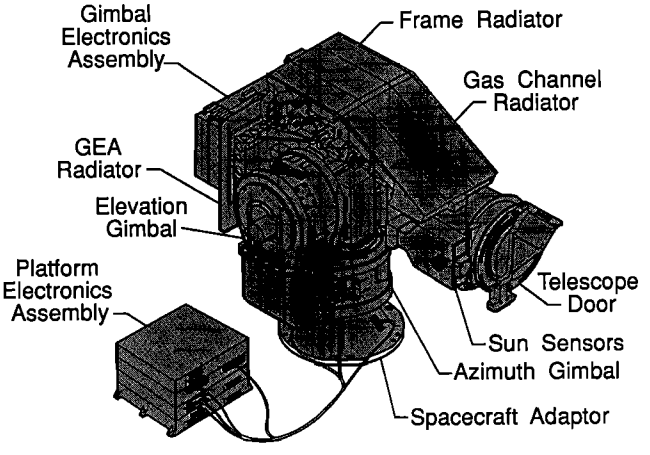

Fig. 11. HALOE instrument configuration.

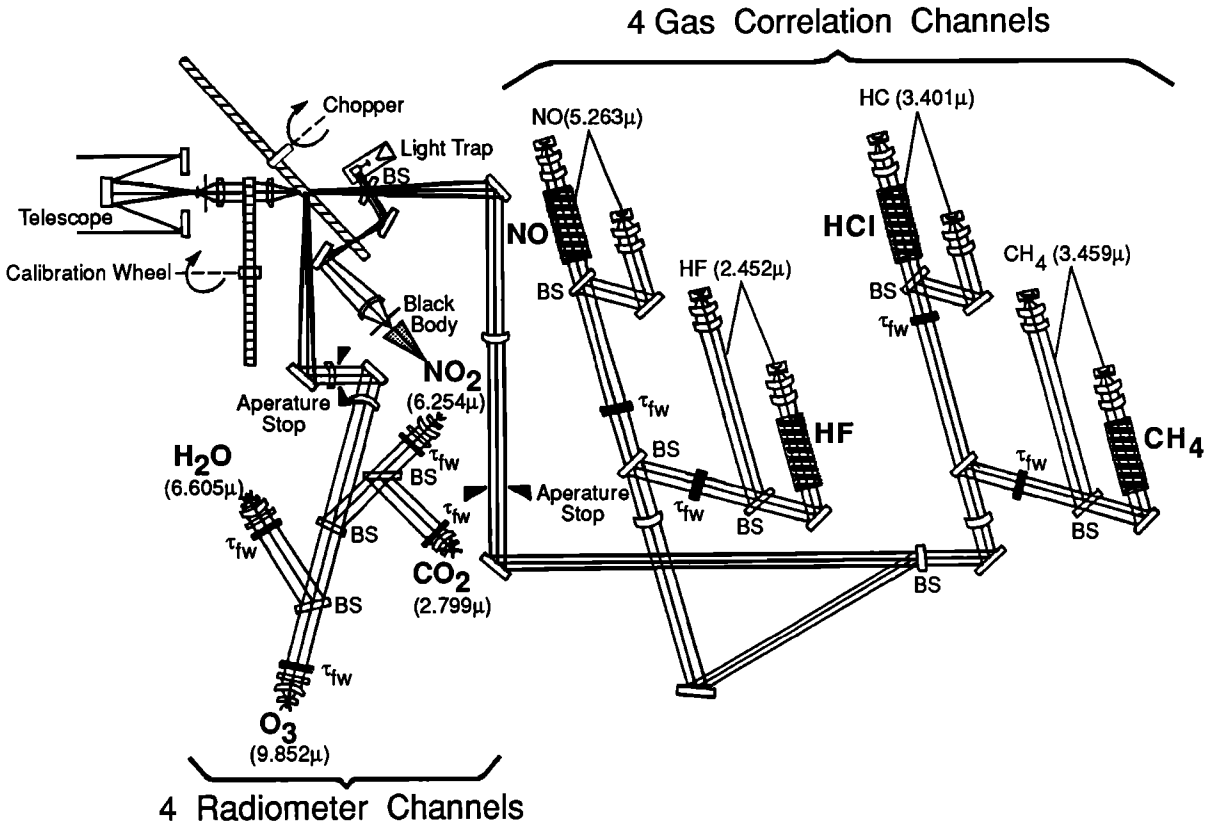

Fig. 12. HALOE optical diagram.

comes to a first focus where a zinc selenide window is located to attenuate the solar UV and minimize contamination effects due to material migrating into the instrument through the telescope path. The energy next passes through a field stop 2 arc min in the vertical by 6.23 arc min in the horizontal. This gives an IFOV at the limb of 1.6 km x 5 km. The field stop is reflective to provide rejection of out-of-field solar energy. The energy is then collimated to allow insertion of a calibration wheel containing 12 ports: an open port which is used for normal data collection, three ports containing neutral density filters with transmissions of approximately 80%, 60%, and 20%, and eight ports containing gas cells (two per channel). This provides scale factor stability checks in orbit for both the radiometer and the gas filter channels. All measurements to date in orbit show scale factor changes of only 1% or less.

The solar energy is chopped at the second focus (≈ 150 Hz) using a blade with regular holes that has been polished and gold-coated on the Sun side to allow the energy to be routed to the broadband radiometer portion of HALOE 50% of the time and to the gas filter section the remaining time. The chopper also modulates energy from the reference blackbody (≈ 300 Hz) mentioned earlier. After the chopper the energy going to the gas filter section is sent through a beam combiner (BC) to bring in energy from the reference blackbody, and then it is recollimated and not focused again until the beam reaches the detectors. The radiometer channel energy is collimated after the chopper and focused later in the train at the detector. The locations of the broadband filters are indicated by solid rectangles with the designation τ_{fw} beside them. Beam splitters are identified by the letters BS. Note the positions of the gas cells in the optical train. The only channel that has other than a reflecting mirror and focusing lenses in the vacuum path is NO. In this case, since sapphire starts to cut off spectrally in the NO band being used, two sapphire gas cell windows were used in the vacuum path to optically balance this effect.

Gas cells and detectors. The gas cells used are gold with sapphire windows for HCl and HF and IN3 glass with sapphire windows for NO and CH_4. The gold cells were built by TRW, Incorporated, in an electroforming processes to obtain high-purity cell walls required to contain the highly corrosive gas HF. Life tests have been under way for 10 years with all instrument and calibration cells filled to flight levels. The stability of the cells in the life-test program have been monitored using high-resolution Fourier transform spectroscopy and nonlinear least squares fit analyses methods. No changes have been observed within the limits of the measurements (≈ 3%, 1σ).

Uncooled immersed thermistor bolometer detectors are used for the four radiometer channels. Each detector assembly uses an antireflective coated germanium dome lens with both an active flake and a compensating flake attached. The detector outputs are arranged in an electronic bridge circuit for signal detection. The compensating flake is used to correct for detector changes due to changes in ambient temperature. Thermoelectrically cooled indium arsenide detectors are used for the HCl, HF, and CH_4 channels, and photovoltaic mercury-cadmium-telluride is used for NO. The nominal operating temperature is about 200 K. Cooling is used more for active temperature control to provide responsivity stability during an occultation event than for improved sensitivity.

Sun sensor. The HALOE Sun sensor subsystem includes two coarse Sun sensors (CSS), a fine Sun sensor (FSS), biaxial gimbal assembly, part of the instrument

microprocessor, and motor drive electronics. The detectors are silicon photodiodes operating in the visible wavelength range. The sensor is used to acquire the Sun, scan the disk, and track the Sun at a fixed point from the top edge during balance, calibration, and science data collection. The gimbals are stepper motor driven with a range capability +11 to -28° in elevation and ± 185° in azimuth. The coarse Sun sensors are analog, and the FSS is digital. The FSS uses a 256-element diode array, which has an angular extent of 1.15°. Spacing between diodes is 16.2 arc sec. The azimuth CSS is used to both acquire and track the radiometric Sun centroid. The elevation CSS is used only to acquire and turn over track control to the FSS after a sign change occurs in the elevation CSS signal. The Sun sensor is boresighted with the infrared telescope during ground tests. This boresight is also routinely checked in orbit. In addition, the Sun sensor threshold used for a beginning or end of event signal can be changed by ground command as can the operating track point relative to the top solar edge.

Orbital calibration and data collection sequences. The normal mode of HALOE operation in orbit is the autosequence described in Figure 13. After solar acquisition on a sunset event, the instrument, under microprocessor control, goes through a ΔV balance sequence. Next, five solar scan cycles are performed to define the HALOE-observed limb-darkening curves in each channel for use in data processing. Upon completion of solar scans the calibration wheel is rotated to check scale factor stability in all channels. This is all completed in 450 seconds so that the instrument is in a science data collection mode by the time the 150-km tangent altitude is reached. The reverse sequence occurs on sunrise except for the balance sequence which is not performed in lieu of a routine Sun sensor alignment check. There are variations to this autosequence which are periodically activated to measure ΔV to V gain values and cross talk, boresight alignment between the infrared telescope and the Sun sensor, field-of-view mismatch, and thermal drift effects.

4.2. Testing and Calibration

Accuracy and precision. Since HALOE makes measurements using both the gas filter and the broadband radiometry techniques, the kinds of errors that affect the measurements are different for different channels. Random errors (affecting precision) common to both methods include instrument noise, pointing angle error, digitization effects, atmospheric temperature uncertainties, and effects of interfering gas mixing ratios that must be inferred from other channels. Sources of certain systematic errors which are common to both experiment approaches include interfering gas effects, atmosphere temperature and reference pressure errors, optical filter characterization uncertainties, linearity errors, errors associated with removal of electronic delays, absorption line strength and half width uncertainties, and errors occurring when the IFOV function is "deconvoluted" from the data.

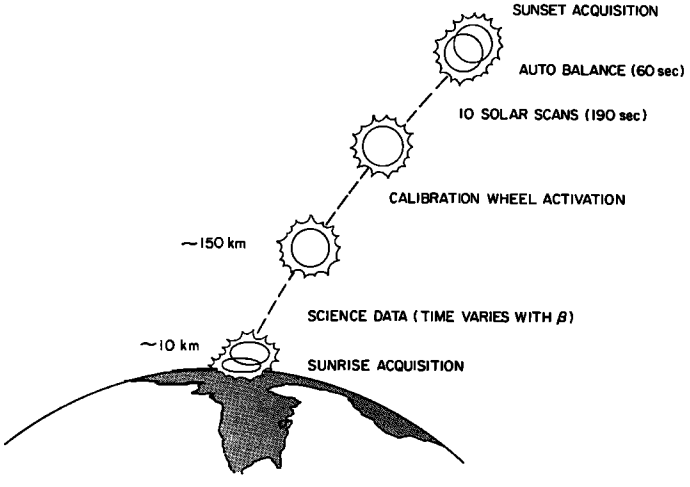

Fig. 13. HALOE normal operational sequence in orbit.

Some additional systematic errors which affect only the gas filter measurements include knowledge of the spectral properties of the gas cell (expressed as an error in cell mass path), errors in the slope of the gas path to vacuum path spectral response ratio, uncertainties in modulation signal drift errors due to strict linearity matching of the two gas filter detectors in each channel, optical cross-talk error, IFOV mismatch uncertainty between gas and vacuum path signals, errors in the ΔV to V gain ratio, errors in the ΔV balance value measured outside the atmosphere, and errors in knowledge of spacecraft velocity used to make corrections for the Doppler effect.

Pointing errors determined in ground testing are 15 arc sec in azimuth and 12 arc sec in elevation. Atmospheric temperature random and systematic errors assumed in studying effects on the experiment are 0.5 K and 3.5 K, respectively. Errors in interfering gas mixing ratios vary from channel to channel but, in general, are of the order of 8% and 20% for random and systematic effects, respectively. The actual values for each channel have been determined by doing retrieval simulations. Absorption line strength and half width errors vary greatly but generally range from about 5 to 10%. The remaining errors which have been estimated based on detailed analysis of laboratory test data are summarized in Table 1.

Spectral response. The HALOE instrument end-to-end spectral response was determined using a specially designed grating monochromator, in combination with a 2800 K solar simulator source. The relative spectral response was measured in every HALOE channel with a spectral resolution ranging from 2 to 4 cm^{-1}. In addition, the spectral properties of the optical filters, characterized as functions of temperature (10°C to 30°C) and angle of incidence using a 0.06 cm^{-1} resolution Nicolet interferometer, were included in the data processing software. Normalized plots of the end-to-end spectral response function for each HALOE channel (vacuum path for the gas filter channels) are shown in Figure 14.

Another spectral element for the gas filter channels is the gas filter cell. The spectra of flight cells installed in HALOE were measured extensively with the Nicolet interferometer, and a nonlinear least squares spectral line fitting program was developed to allow inference of the optical mass path that gives the best fit to the spectral line structure observed with the interferometer. This approach provided an essentially infinite resolution characterization of the gas filter portion of the spectral response.

Spatial response. The optical field of view (FOV) for each HALOE channel was measured by scanning a knife edge and a narrow slit (10% of the FOV width) between HALOE and a solar simulator source and by scanning the IFOV across the surface of the actual Sun from the ground. The primary parameters characterized in these tests were the normalized

Table. 1 HALOE Error Sources and Magnitudes

Error Type	Magnitude							
	HCℓ	HF	CH_4	NO	CO_2	NO_2	H_2O	O_3
			Random Errors					
Noise	0.2 nem	0.4 nem	0.6 nem	0.3 nem	0.0003	0.00057	0.00023	0.00023
Digitization								
modulation	0.09/τ	0.09/τ	0.35/τ	0.09/τ	–	–	–	–
transmission τ	$2x10^{-4}$ x M/τ	$2x10^{-4}$ x M/τ	$8.5x10^{-4}$ x M/τ	$2x10^{-4}$ x M/τ	0.00023	0.00023	0.00023	0.00023
			Systematic Errors					
Atmos. ref. press††	2.3%	2.3%	2.3%	2.3%	–	2.3%	2.3%	2.3%
Gas filter cell mass path	2%	2%	2%	2%	–	–	–	–
Spectral filter								
gas/vac slope	0.3%/100 cm^{-1}	0.3%/100 cm^{-1}	0.3%/100 cm^{-1}	0.3%/100 cm^{-1}	–	–	–	–
filter spread+ % of value	20%	–	20%	20%	2%	–	–	–
filter shift † % of value	10%	10%	10%	10%	3%	100%*	10%	10%
filter slope	1%	1%	1%	1%	1%	1%	1%	1%
random spectral response	0.3%	0.3%	0. 3%	0.3%	1%	1%	1%	1%
Doppler shift correction	1%	1%	1%	1%	–	–	–	–
Electro-optical								
modulation drift/min	0.11 nem	0.11 nem	0.11 nem	0.11 nem	–	–	–	–
linearity	$0.7x10^{-4}$ x (1-τ)	$0.4x10^{-4}$ x (1-τ)	$0.5x10^{-4}$ x (1-τ)	$1.2x10^{-4}$ x (1-τ)	< 8 x 10^{-5}	< 8 x 10^{-5}	< 8 x 10^{-5}	< 8 x 10^{-5}
solar-to-reference cross talk								
ΔV	10^{-3} x M	$3x10^{-3}$ x M	$5x10^{-3}$ x M	$0.4x10^{-3}$ x M	–	–	–	–
V	$0.6x10^{-4}$ x τ	$0.4x10^{-4}$ x τ	$0.7x10^{-4}$ x τ	$0.6x10^{-3}$ x τ	–	–	–	–
balance offset	0.09 nem	0.09 nem	0.35 nem	0.09 nem	–	–	–	–
ΔV to V gain	0.0017 x M	0.0017 x M	0.0017 x M	0.0017 x M				
			Spatial Errors					
Fov mismatch	0.0009 x dτ/dz	0.0018 x dτ/dz	0.0009 x dτ/dz	0.00135 x dτ/dz	–	–	–	–
Electronics and Fov deconvolution	< 3 nem	< 3 nem	< 3 nem	< 3 nem	–	–	–	–

Nem, noise equivalent modulation; Fov, field-of-view.
*Even though the error is large, the shift is extremely small.
+Error in coefficient describing spread in spectral filter width as a function of temperature.
†Error in coefficient describing shift in spectral filter center wavenumber position as a function of temperature.
††Corresponds to 150 m uncertainty.

IFOV function, the FOV mismatch between the gas and the vacuum path IFOV functions, and the degree of off-axis rejection. The most sensitive parameter of these three is the FOV mismatch which must be known to a high accuracy. Fortunately, this parameter can be measured both in the laboratory and in orbit with sufficient accuracy. Test results obtained from knife edge and solar scans show that the centers of the two FOVs differ by, at most, < 0.3 arc seconds in the worst case. The IFOV function for HF, which is typical of the other channels, is shown in Figure 15. The off-axis rejection properties of the four gas filter channels and the ozone channel were measured during the "Sun look" test, and properties for all channels have been measured in orbit. Performance in orbit meets or exceeds requirements at all IFOV positions but by more than an order of magnitude when the IFOV center is 6 arc min from the solar edge.

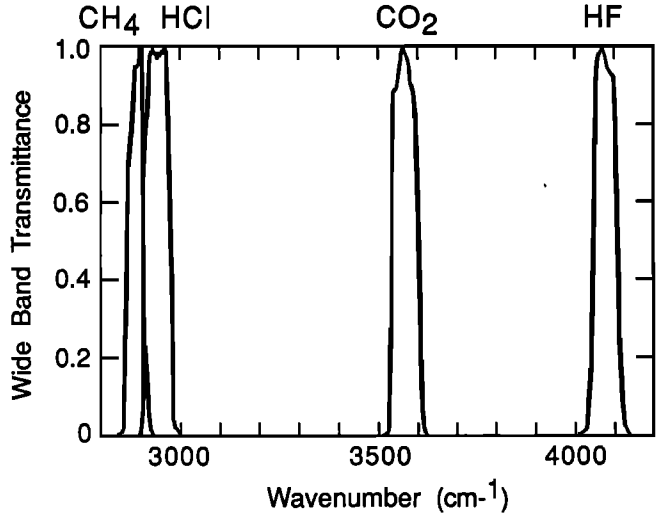

Fig. 14*a*. HALOE broadband end-to-end spectral response for the CH_4, HCl , CO_2, and HF channels.

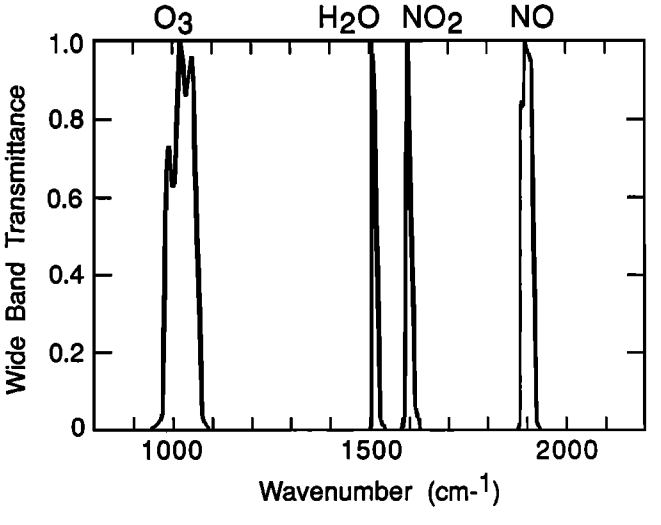

Fig. 14*b*. HALOE broadband end-to-end spectral response for the O_3, H_2O, NO_2, and NO channels.

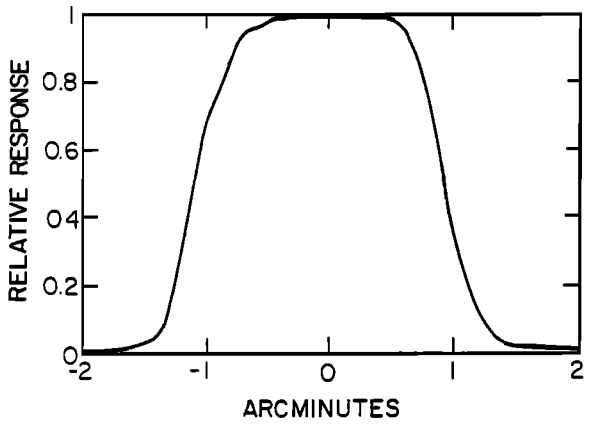

Fig. 15. HALOE HF channel normalized field-of-view function.

Electronics response. Amplitude distortion and phase delay caused by the HALOE electronics have been accurately measured by conventional electronic techniques. The resulting response versus frequency plots have been analyzed and show that the four-pole Butterworth filter expression in Fourier space

$$\beta(\omega) = \left[(\omega_m^4 - A\,\omega_m^2 + 1) - (B\omega_m^3 - C\,\omega_m)\,i\right]^{-1} \quad (9)$$

represents the frequency response of the instrument to the 1-2% level. In this expression, $\omega_m = 2\pi\omega/D\omega_B$, where ω_B = 0.91 Hz, A=3.67, B=2.774, C=2.840, D=7.3086, and $i = \sqrt{-1}$. The quantity ω is frequency. As a test of this expression, a knife edge test was done after the instrument was integrated on the spacecraft, and the resulting end-to-end "impulse" response was compared with the predicted response using equation (9). The comparison verified that (9) provides an excellent representation of the time response; consequently, any distortion due to uncorrected error from this source will be very small in the total experiment.

Optoelectronic linearity. Optoelectronic linearity is of particular interest for the gas filter channels since the detector response as a function of solar signal on each detector must be closely matched. The electronics response must be matched as well. The end-to-end linearity of the HCl, HF, and CH_4 channels was determined during the ground "Sun look test" by placing wire grid attenuators of known transmission in front of the HALOE telescope while viewing the Sun. Attenuators of approximately 10%, 20%, and 50% were used. Insufficient signal existed to determine NO linearity in this test. The grids were rotated in place through angles of 60° and 120° to test for polarization effects and none were found. The requirement is that the deviation in ΔV, due to nonlinearity, be a small fraction (< 1%) of ΔV itself. Tests showed that this requirement was met or exceeded in all gas filter channels. Ground tests show that this nonlinearity is a very small error source for the radiometer channels and can be neglected.

Thermal sensitivity. Thermal sensitivity of signals in HALOE can arise from two main sources. The optical broadband interference filter characteristics, for example, are temperature dependent, as already noted. Also, thermal changes will induce small optical misalignments due to thermomechanical stresses on the optical mainframe. The former is the main source of thermally induced signals in the bolometer channels, and the latter is the principal factor in the gas filter channels. In addition, the gas filter detectors have temperature dependent responsivities, but this effect is small since they are held at a constant temperature (to ≤ 0.01 K) by thermoelectric coolers. The gas filter channels are the greatest concern because of the small radiance differences being observed. As already noted in section 2, an empirical fit approach which employs data obtained just prior to sunset or after sunrise is being used to model drift rate and to correct the orbital data.

Estimated errors. The effect of all experiment errors on estimated uncertainties in retrieved parameters was studied using a Monte Carlo simulation in combination with the onion peeling retrieval approach. The study was based on the errors in Table 1 and other sources of uncertainty discussed previously. An alternate error estimation approach has also been studied using the analysis technique developed by Rodgers [1990]. Our preliminary estimate of the single-profile precision over the 20- to 35-km range is 3 to 8%, depending on channel, and the zonal mean profile precision is estimated to be 2 to 5%. Accuracies (combination of random and systematic errors) are estimated to be 2 to 3 times the precision values. A detailed description of error studies performed and data limitations is provided in a series of validation papers in preparation.

Gas response test. The culminating HALOE ground test was the end-to-end gas response test (GRT). The purpose of this test was to create a simulated atmosphere in front of the HALOE instrument using gas cells to vary the type, mixing ratio, and pressure of gas in the cells; then to record the HALOE signals; and, finally, to compare calculated signals with the measurements. The calculated signals were determined from first principles using the flight software and key properties of the instrument characterized in laboratory testing. No empirical adjustments or parameterized calibration fits were used in the calculations. The instrument was placed in a thermal/vacuum chamber so that its temperature could be controlled. A test apparatus was constructed containing the simulated atmosphere gas cells that could be moved in place outside the chamber, optically aligned, and the apparatus purged with dry nitrogen to remove or reduce residual laboratory air so that absorption (especially due to water vapor and CO_2) was at a minimum. The test apparatus contained a 2800 K solar simulator source, optics, and two gas cells, one of which could be used to create a target gas "atmosphere" and the other to provide the simultaneous presence of interfering gases. Mixing valves were built into the system so that various N_2-gas mixing ratios and total pressures could be achieved. Ranges of mixing ratio and pressure were preselected to simulate, to the extent possible, limb path signal levels that would be measured by HALOE in orbit. In some cases, manufacturer-supplied premixed gases were used. The mass paths of gas in the simulated atmosphere cells were determined both by pressure gauge readings and by spectral analysis using high-resolution Fourier transform spectroscopy. The greatest problem encountered was in handling and determining how much HF was in the cell at any given time. After a significant amount of study, satisfactory results were obtained. Typical results for HCl and HF are shown in Figure 16 for a 20°C HALOE instrument temperature. The GRT was done for three instrument

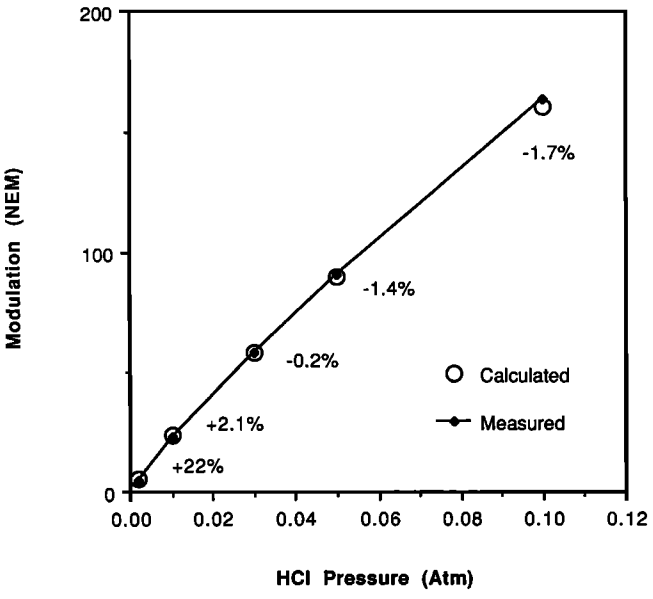

Fig. 16*a*. HALOE HCl gas response test (GRT) results for 20°C instrument temperature.

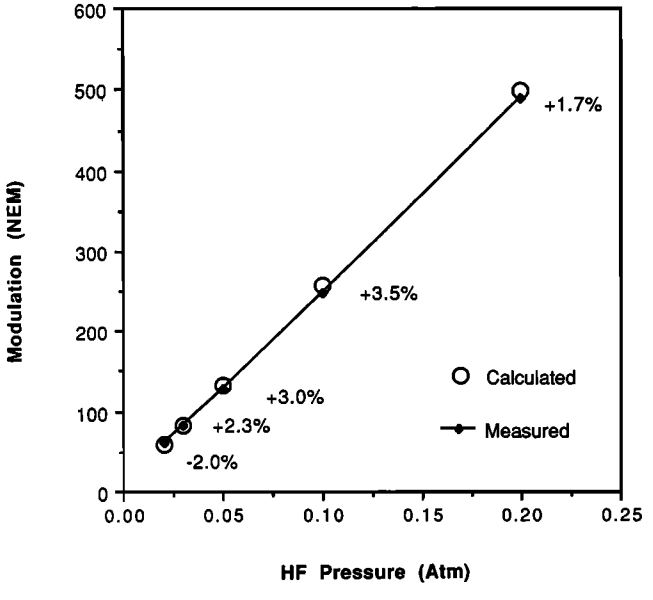

Fig. 16*b*. HALOE HF GRT results for 20°C instrument temperature.

temperatures (10°C, 20°C, and 30°C) spanning the range of expected orbital values. The HCl and HF observations (diamonds) and calculations (circles), along with differences in percent, are shown. In most cases, agreement to less than a few percent was obtained. The only exception was for the lowest HCl signal, and while the difference is large here, it represents less than one step in the HALOE digitizer system. Also, at these low pressures, pressure gauge errors will have a larger effect, and the amount of HCl in the cell is more uncertain. Differences obtained for CH_4 and NO were of the order of a percent or less. These results hold at all three instrument temperature test conditions for CH_4 and NO and at 20°C and 30°C for HCl and HF. At 10°C instrument temperature the differences grow to 2-10% for HCl and 3-8% for HF. The reasons for this are under investigation, but this is not so important since the orbital instrument temperature never drops below 20°C.

The most reliable radiometer channel for study of agreement between measurements and calculations is CO_2. In this case, calculated transmittances agreed with observed values to within 2-3%. Comparisons were also made for the NO_2, H_2O, and O_3 transmittances. In these cases, agreement was much worse, 4-40% (the largest difference was for O3), and we attribute this to gas-handling problems. Since the radiometer measurements are simple in concept and CO_2 agrees well, no further effort was expended to reduce differences.

An initial GRT was done in 1989, then the instrument was shipped to the spacecraft manufacturer for the first series of integration activities, and in 1990, HALOE was shipped back to the Langley Research Center for final testing, including a repeat GRT. Similar results to the first GRT were obtained. Also, a comparison was made between 1989 and 1990 GRT measurements for the same target cell pressures to assess the repeatability of the instrument/GRT system. This would be an upperlimit determination of instrument repeatability since the repeatability of the test setup is also included. The agreement for 20° instrument temperature between the 1989 and 1990 measurements for the same mixing ratio and pressure test points was of the order of 1% for CH_4 and 2-4% for HCl and NO. This could not be done for HF because HF gas-handling problems which were encountered in the 1989 test improved in 1990.

The GRT results attest to the quality and degree of characterization of the HALOE instrument, and they lend confidence that the instrument is well understood. The precision indicated by the GRT measurements suggests that the HALOE measurement repeatability when viewing the same atmosphere is better than 1-4%. The comparison between measurements and calculations show that when the atmospheric pressure, temperature, and gas mixing ratio parameters are known, the measured HALOE signal can be predicted to within a few percent using the flight software.

4.3. In-Orbit Instrument Performance

The HALOE instrument has been operating continuously since science observations began on October 11, 1991, except for periods when two grazing events occurred: one shortly after operations started and the other near the end of December. A grazing event is a time when either the Sun does not set at the spacecraft or the dark period is very short and the lowest measurement tangent point is very high, e.g., > 90 km. The instrument performance has been essentially flawless. In all cases the orbital performance meets or exceeds specifications. The radiometer channel equivalent transmittance noise is < 0.05%; the gas filter channel modulation noise is ≈ 0.2 NEM for HCl and HF, 0.5 NEM for CH_4, and 0.7 NEM for NO. Modulation drift rates are < 0.3 NEM/min for HCl and HF, < 0.6 NEM/min for NO, and < 1 NEM/min for CH_4. The FOV mismatch observed in orbit is ≈ 0.3 arc sec. The off-axis rejection properties of the instrument show < 0.1% of full Sun signal when the IFOV center is 4 arc min off the solar edge.

A major challenge to the operation of HALOE in orbit has been the effect of the Mount Pinatubo aerosol layer on the pointer/tracker system. This layer is very dense, and HALOE

data show that it extends over a broad altitude range from 28 km down to 16 km in places. The extinction is so large that the Sun sensor magnitude threshold value used to signal the beginning or end of an event becomes nearly zero at 25 to 28 km altitude, depending on geographic location. After considerable study of the orbital data, fine adjustment was made to the Sun sensor threshold value to increase the useful altitude range. The value is now set at 0.1% of full Sun signal for sunset and 0.5% for sunrise. Changes were also made to the pointer/tracker sunrise acquisition algorithm to decrease the time required for solar acquisition. The IR telescope tracking lock point on the Sun is changed routinely depending on latitude from 4 arc min to 8 arc min down from the top edge. These changes provide altitude coverage in the worst case dense aerosol condition down to about 20 km. Most of the time the coverage is of the order of 5 km or more lower than this, and it should continue to improve with time as the aerosol extinction subsides. The pointer/tracker has the capability to track down to the solid Earth point on sunset and acquire and begin track above about 5 km on sunrise under background aerosol conditions. The performance of the pointer/tracker has met specifications throughout the mission.

5. Data Processing and Inversion Approach

5.1. Level 0-1 Processing

This stage of processing unpacks the HALOE level 0 or raw data, calibrates the data, removes instrument effects, develops source functions from the solar scan data, and registers the data with pressure and altitude. Registration is done by using an NMC temperature versus pressure profile to do a CO_2 channel signal simulation and then by comparing the simulation to measurement. The altitude range above 30 km is used to avoid any serious effects due to aerosol contamination. The unpacking separates the data into files that correspond to various instrument modes. These data are then processed on the UARS Central Data Handling Facility (CDHF) at the Goddard Space Flight Center and transmitted to the HALOE remote access computer (RAC) for detailed analysis. The level 0-1 processing therefore provides a set of corrected and calibrated signals that are ready for retrieval calculations.

5.2 Level 1-2 Processing

This step uses transmission profiles, difference signal profiles from the gas filter channels, and solar source functions from the solar scans to retrieve temperature, pressure, and mixing ratios of HCl, HF, CH_4, H_2O, O_3, NO, NO_2, aerosol extinction, and temperature versus pressure. We are retrieving temperature only above $\approx$ 30 km at present because of effects due to aerosol contamination. The retrieval method incorporates a simple "onion peel" procedure stabilized at the top and bottom of the profile with a scalar optimal estimation formulation [Connor and Rodgers, 1989]. The forward model for the gas filter channels (HF, HCl, CH_4, NO) is a rigorous line-by-line code which is necessary for the effective high spectral resolution of these channels. All spectral dependence, including thermal and Doppler shift effects, is explicitly modeled. Along-path mixing ratio gradients are also included in the forward model for the diurnally active gases NO, NO_2, and O_3.

The radiometer channels are modeled using the emissivity growth and Curtis-Godson approximations using correction tables. These models have been validated against a line-by-line transmission code to better than 99% accuracy, and they are extremely fast, allowing a vector implementation of the optimal estimation equations. Again, full thermal and spectral dependence of the instrument is rigorously modeled, in this case, through a large set of transmission tables.

Most major interfering gases are retrieved as primary gases in other channels. Nonretrieved interference is minor (such as N_2O in HCl) contributing <1% error. However, interference from the Mount Pinatubo aerosol layer causes a major effect on the radiometer channel retrievals below the top of the aerosol layer. We have devised a correction approach which is based on retrieval using the gas filter channels, coupled with a Mie-scattering model to determine the aerosol extinction at the radiometer channel wavelengths [Hervig et. al. 1993]. This approach works very well based on comparison with correlative measurements. After correction for aerosol interference, HALOE O_3 and H_2O data agree well with correlative measurements to within about 10-15%. No correlative data are yet available for NO_2.

5.3. Level 2-3 Processing

The primary level 3 or "mapped" products from HALOE include pressure versus longitude cross sections on selected days, pressure versus latitude for selected time periods, and polar orthographic projections. The latitude cross sections are generated on time scales of a couple of weeks or more and seasonally. The accuracy and precision of these products are high and therefore they provide very reliable means to study trends over time.

6. HALOE Data Validation

An extensive effort is underway to validate the HALOE measurements. The first-order evaluation has been a qualitative check of profile shapes and latitudinal changes. In all cases the profile shapes, magnitudes, and latitudinal variations are within reasonable bounds. We have also performed internal consistency checks such as evaluation of sunrise/sunset differences to verify that those gases that do not vary diurnally (i.e., stratospheric O_3, H_2O, CH_4, HCl, HF) are not changing and those that should be changing (NO, NO_2) vary within reasonably expected limits. Examples of these results are shown in Figure 17 for January 29, 1992, when sunrise and sunset observations overlapped in the tropics. This is a good region for study since atmospheric changes due to dynamics should be relatively small. The figures show both the lack of change and the expected diurnal differences.

Another internal consistency check is regression analyses of long-lived parameters against each other to verify strong correlation when both are dynamically controlled and, in the case of H_2O versus CH_4, to determine if the slope of the regression is in accord with methane oxidation theory. Scatter plots of HF versus CH_4 and H_2O versus CH_4 are shown in Figures 18 and 19, respectively. Note the strong correlations illustrating the utility of these parameters as tracers. The slope of a least squares straight line fit through the H_2O versus CH_4 data is about 2.0, in good agreement with the expected slope, based on oxidation of methane. The slope of the HF versus CH_4 regression is 1.0.

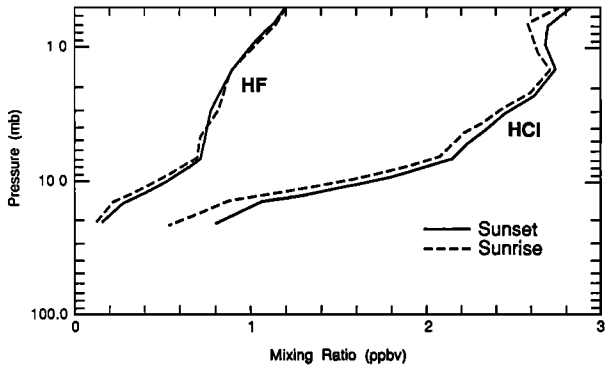

Fig. 17*a*. HALOE zonal mean HF and HCl mixing ratios, sunrise, and sunset on January 29, 1992, at 20°N.

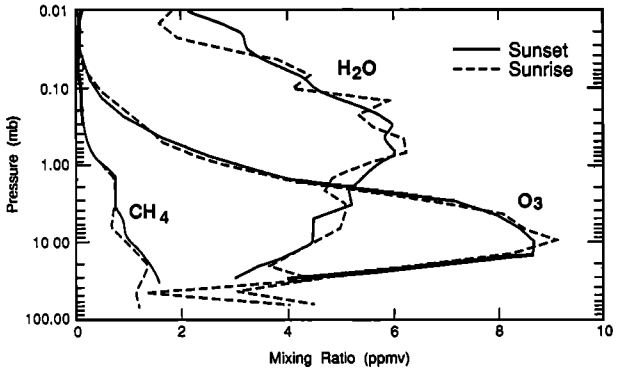

Fig. 17*b*. HALOE zonal mean O_3, H_2O, and CH_4 mixing ratios, sunrise, and sunset on January 29, 1992, at 20°N.

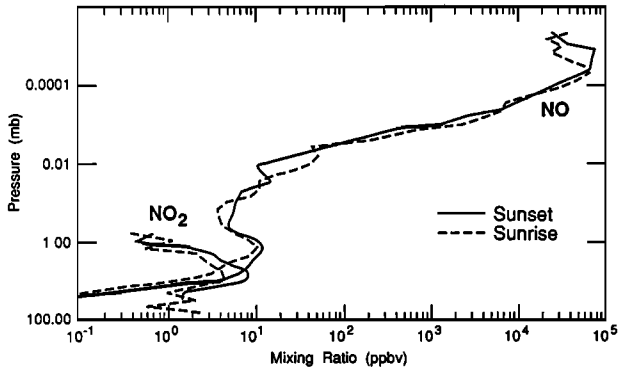

Fig. 17*c*. HALOE zonal mean NO and NO_2 mixing ratios, sunrise, and sunset on January 29, 1992, at 20°N.

An important step in the data validation is comparison with correlative underflight data. The most abundant HALOE correlative set is for O_3, which has been measured from the ground using microwave techniques and lidar, from aircraft using in situ methods, and from balloons using the electrochemical concentration sonde. The next most plentiful correlative data set is H_2O, which has been measured from aircraft and balloons, followed by HCl from both platforms, and NO measured from aircraft. There have also been a few HF profiles measured from balloons to date. At present, the correlative data base is growing, but results are still in an early stage, and comparisons will not be shown. These comparisons will be described in the HALOE data validation papers now in preparation. Qualitative comparisons of zonal mean results on May 7 with 1985 Spacelab 3 (ATMOS) zonal mean data [Farmer et al., 1987] are shown in Figure 20. ATMOS was launched in late April 1985 and made measurements of all parameters observed by HALOE. Because of the vast time differences, quantitative agreement is not expected. Also, the latitudes for the two data sets differ by 5°, which could introduce biases. The expected increase in HF is shown by the comparisons (about 5 to 6% per year), and the profile shapes compare well for the two data sets. The HCl increase shown by HALOE, however, is less than might be expected. The causes for this are under investigation and will be discussed in detail in the HCl validation paper in preparation. The other parameters are all in reasonable agreement considering the vast time differences between the two data sets. Based on these comparisons and early results from the correlative data, we conclude that the HALOE data set is of good quality and is very useful for carrying out scientific investigations.

7. HALOE Results

A set of pressure versus latitude trace gas and aerosol sunset cross sections for the period September 21 to October

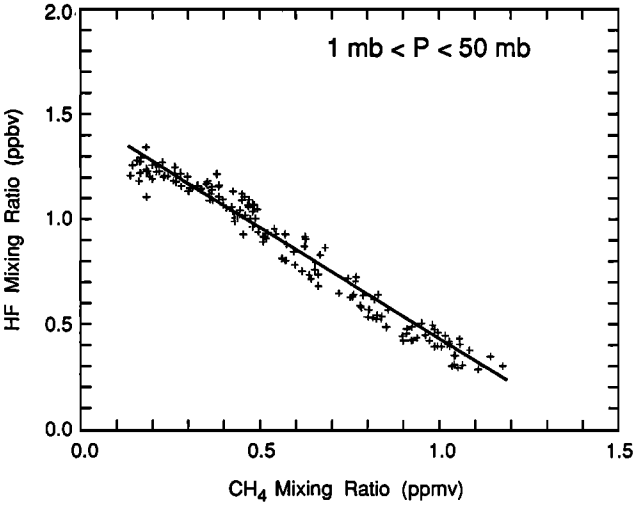

Fig. 18. HALOE HF mixing ratio versus CH_4 mixing ratio, sunset on January 23, 1992, at 53°N, 248°E.

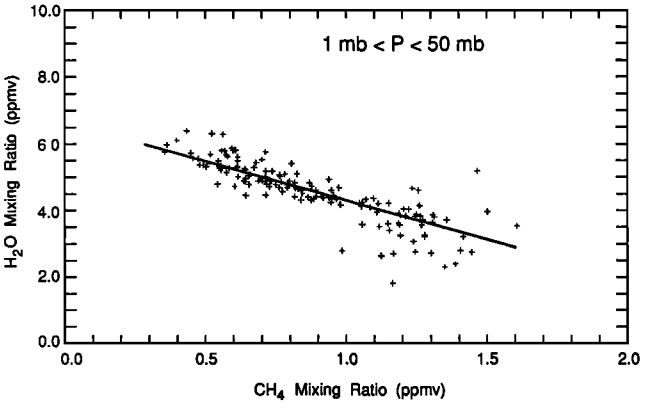

Fig. 19. HALOE H_2O mixing ratio versus CH_4 mixing ratio, sunset on January 30, 1992, at 19°N, 260°E.

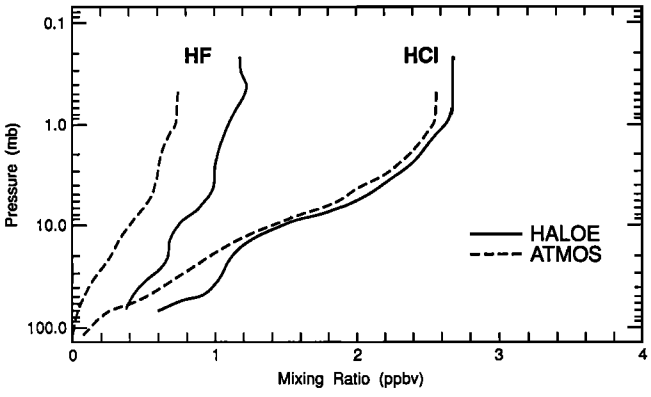

Fig. 20*a*. HALOE HCl and HF mixing ratio on May 5, 1992, at 34°N and ATMOS on May 5, 1985, at 29°N.

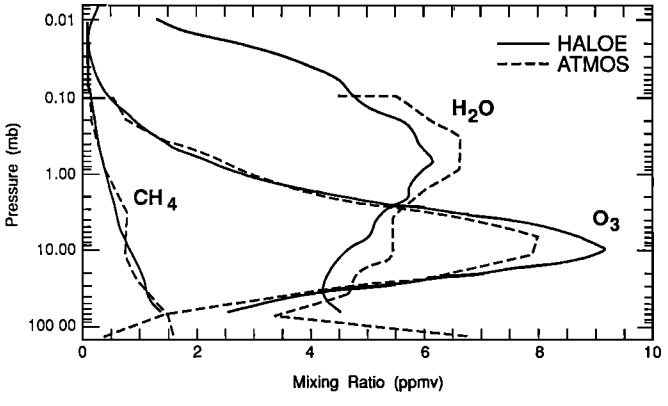

Fig. 20*b*. HALOE CH_4, H_2O, and O_3 mixing ratio on May 7, 1992, at 34°N and ATMOS on May 5, 1985, at 29°N.

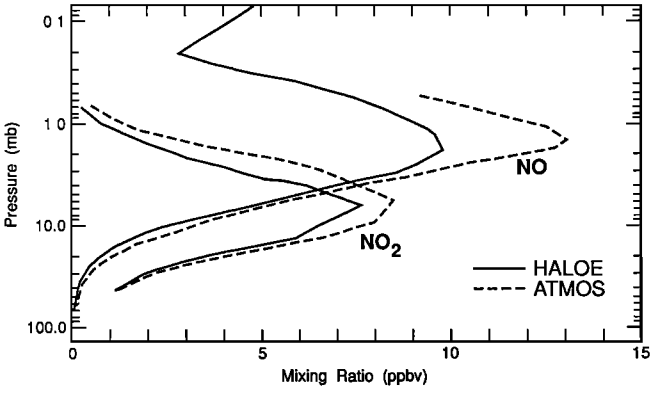

Fig. 20*c*. HALOE NO and NO_2 mixing ratio on May 7, 1992, at 34°N and ATMOS on May 5, 1985, at 29°N.

15, 1992, are shown in Plates 1-8. The measurements started at ≈ 60°N on September 21 and progressed down in latitude to ≈ 80°S on October 15. Approximately 340 profiles per parameter were collected during this time period. Each profile was treated as an individual observation in constructing the cross sections. The cross section was generated using a Gaussian-averaging function with a 1σ of 3° in latitude, and results were plotted at 1° latitude grid spacing. The averaging was truncated at the 2σ point. Since it takes 24 days to cover the latitude region shown, the figures do not represent a true zonal mean. They are useful, however, in giving a good latitudinal picture to the extent that the mean atmosphere does not change appreciably over this time period.

The period selected covers the Antarctic spring when the ozone hole was in its development and stable or recovery phase. Cross sections for CH_4, HF, and H_2O are shown in Plates 1, 2, and 3, respectively. The data at the top of the plate show how the measurement sampling progressed with time. These data show several characteristics that should be noted. First, the cross-section features exhibit striking similarities and demonstrate internal consistency which further supports their validity. All are long-lived tracers. Note the high CH_4, low HF, and low H_2O in the Tropics, consistent with Hadley cell upwelling. Also, the shapes of the contours are similar throughout the stratosphere. All three molecules display evidence for unmixed descent in the south polar region. The CH_4, for example, has a virtually constant and low mixing ratio from the lower mesosphere down to about 25 km. This result is discussed by Russell et. al. [1993] in a separate paper. The H_2O cross section shows the Antarctic dehydration, the tropical hygropause, and a continuous region of low water vapor throughout the lower stratosphere of the southern hemisphere [see Tuck et.al., 1993]. Also, the H_2O mixing ratio reaches a peak just above the stratopause at about 6.2 parts per million by volume (ppmv), then declines up to the limit of the HALOE observations at ≈ 80 km (0.01 mbar).

The HCl cross section is shown in Plate 4. Below the 20-mbar level it shows low values in the tropical lower stratosphere and poleward slope features that are similar to the HF cross section, suggesting that dynamical control is occurring. The middle to upper stratosphere does not show characteristics seen in the three tracers. The midstratosphere HCl shows a hemispheric asymmetry with higher mixing ratios occurring in the south at this time.

The ozone cross section in Plate 5 shows the expected maximum in the equatorial mid stratosphere of ≈ 11 ppmv, and the data suggest that poleward transport is occurring as indicated by the pointed contour slopes above 10 mbar, especially in the south. The effect of the ozone hole can be seen in the south polar region as well. The data do not show much evidence of the tropical upwelling seen in the tracer molecule cross sections.

The NO and NO_2 cross sections are shown in Plates 6 and 7. The NO results extend up to at least 130 km (10^{-5} mbar). The NO mixing ratio has very low values in the lower stratosphere at all latitudes (< 0.25 ppbv). It increases to a stratospheric peak of ≈ 10 ppbv, decreases to a minimum in the lower mesosphere, and then increases sharply with altitude up to the limit of the observations. We also note that correlations with solar activity have been clearly seen, especially during the geomagnetic storm of November 8-10, 1991, a time period when enhanced charged-particle production occurred. The data show that during this period, NO levels in the 80-km to 130-km range increased by a factor of 3 and then decayed to previous levels after only a few days. The NO_2 cross section shows a maximum sunset mixing ratio at ≈ 8 mbar of ≈ 10 ppbv and a hemispheric asymmetry (larger values to the south). Equatorward gradients are observed in both hemispheres. The NO_2 level is low in the lower stratosphere (< 1 ppbv) at all latitudes. The mixing ratio levels also decrease and reach the HALOE noise limit near or just

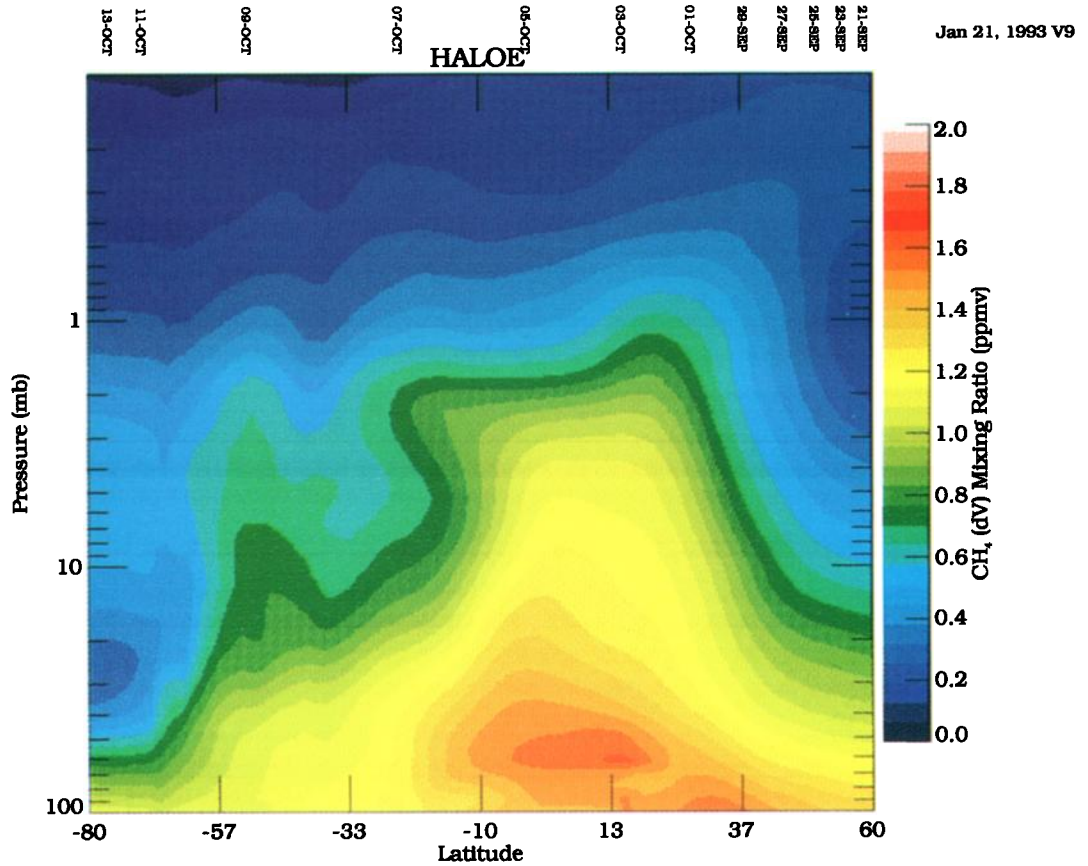

Plate 1. HALOE CH_4 pressure versus latitude cross section, sunset for September 21 to October 15, 1992.

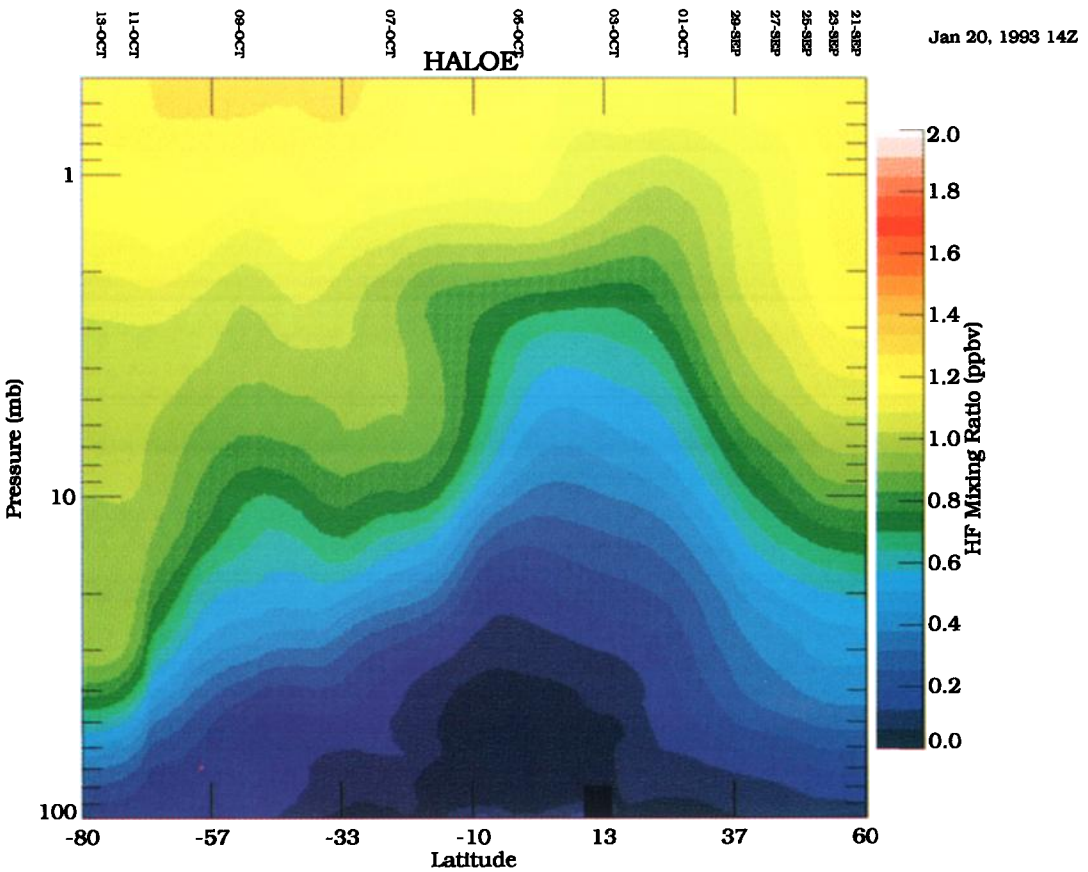

Plate 2. HALOE HF pressure versus latitude cross section, sunset for September 21 to October 15, 1992.

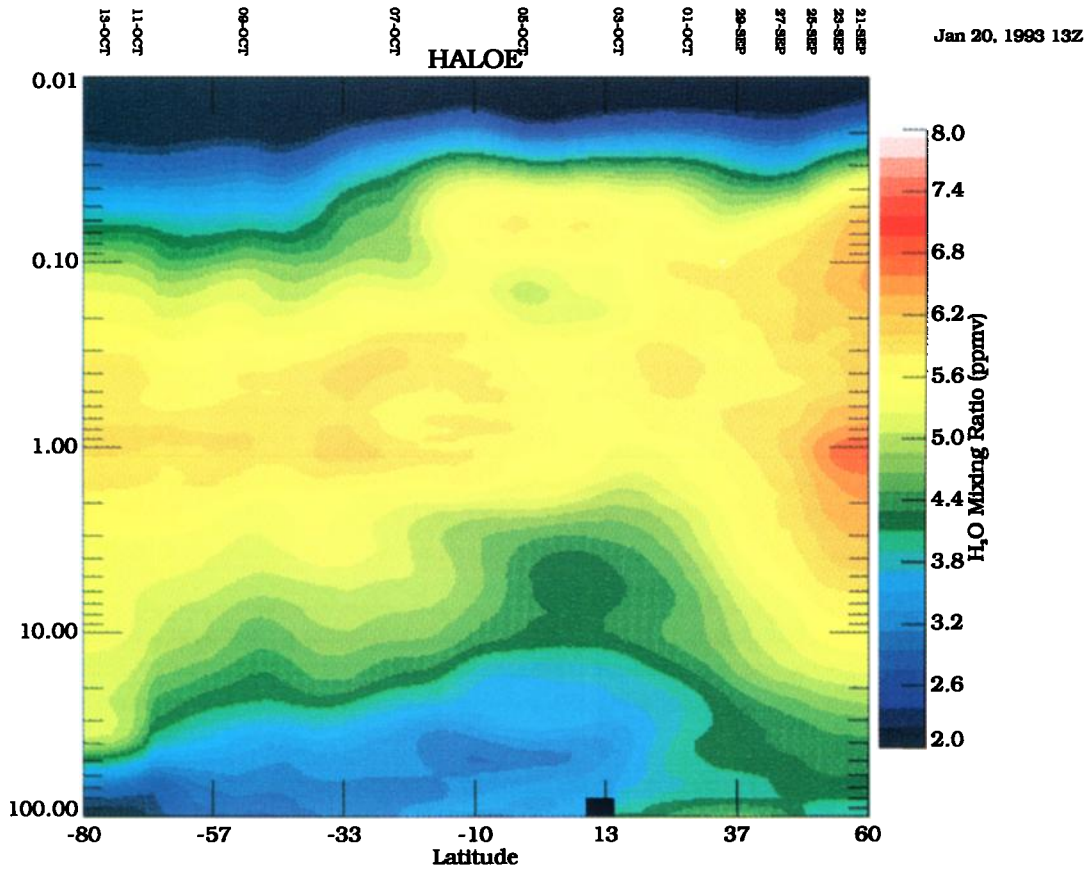

Plate 3. HALOE H_2O pressure versus latitude cross section, sunset for September 21 to October 15, 1992.

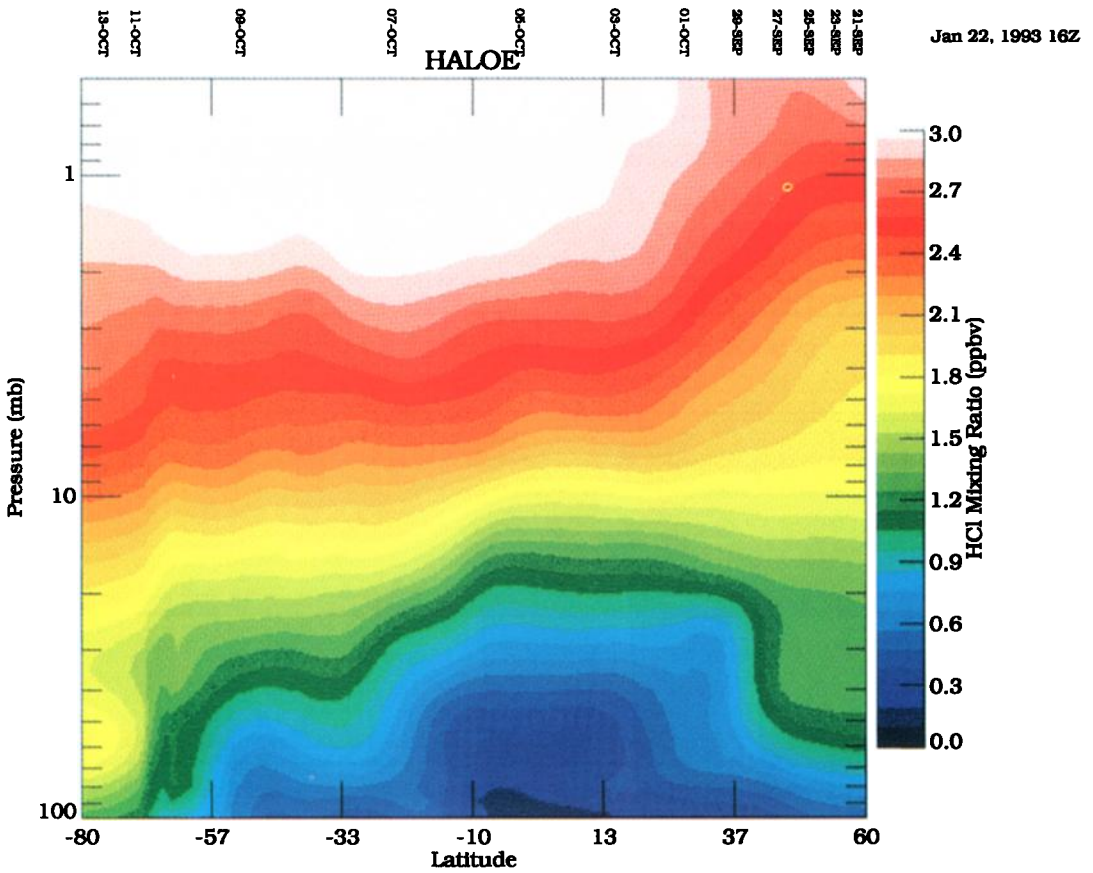

Plate 4. HALOE HCl pressure versus latitude cross section, sunset for September 21 to October 15, 1992.

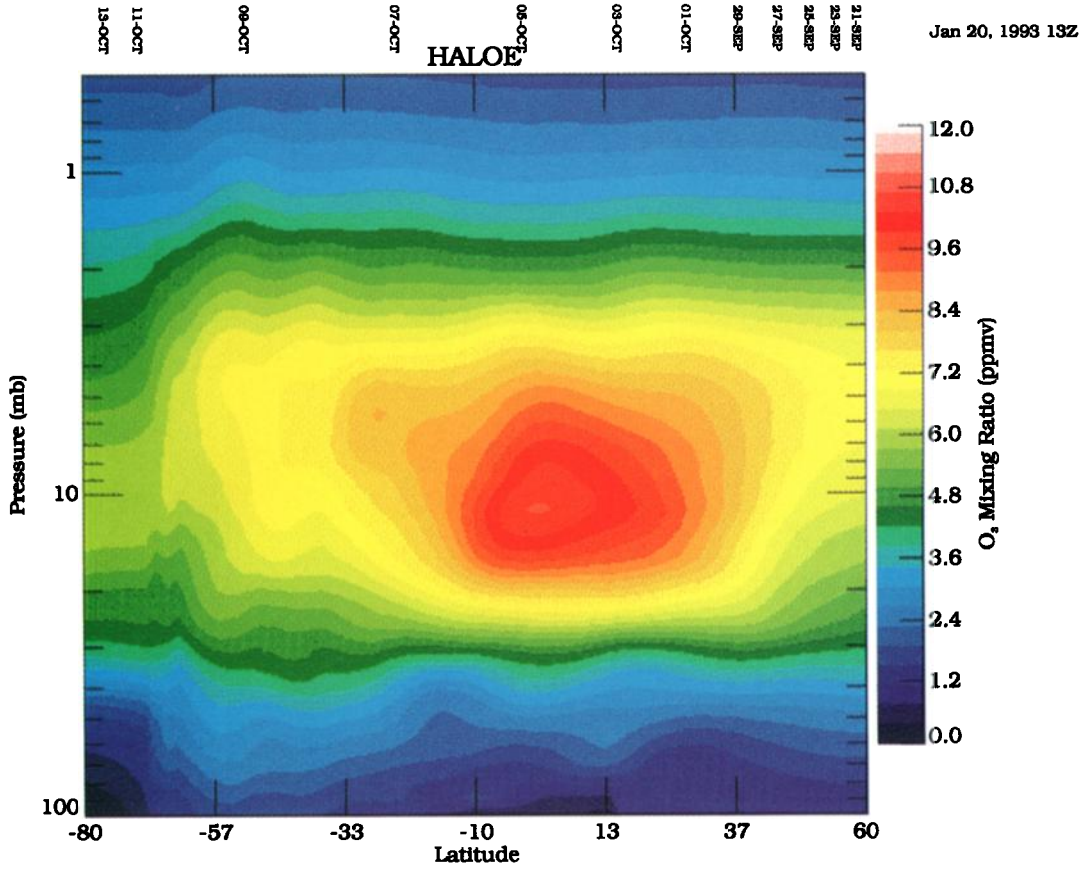

Plate 5. HALOE O_3 pressure versus latitude cross section, sunset for September 21 to October 15, 1992.

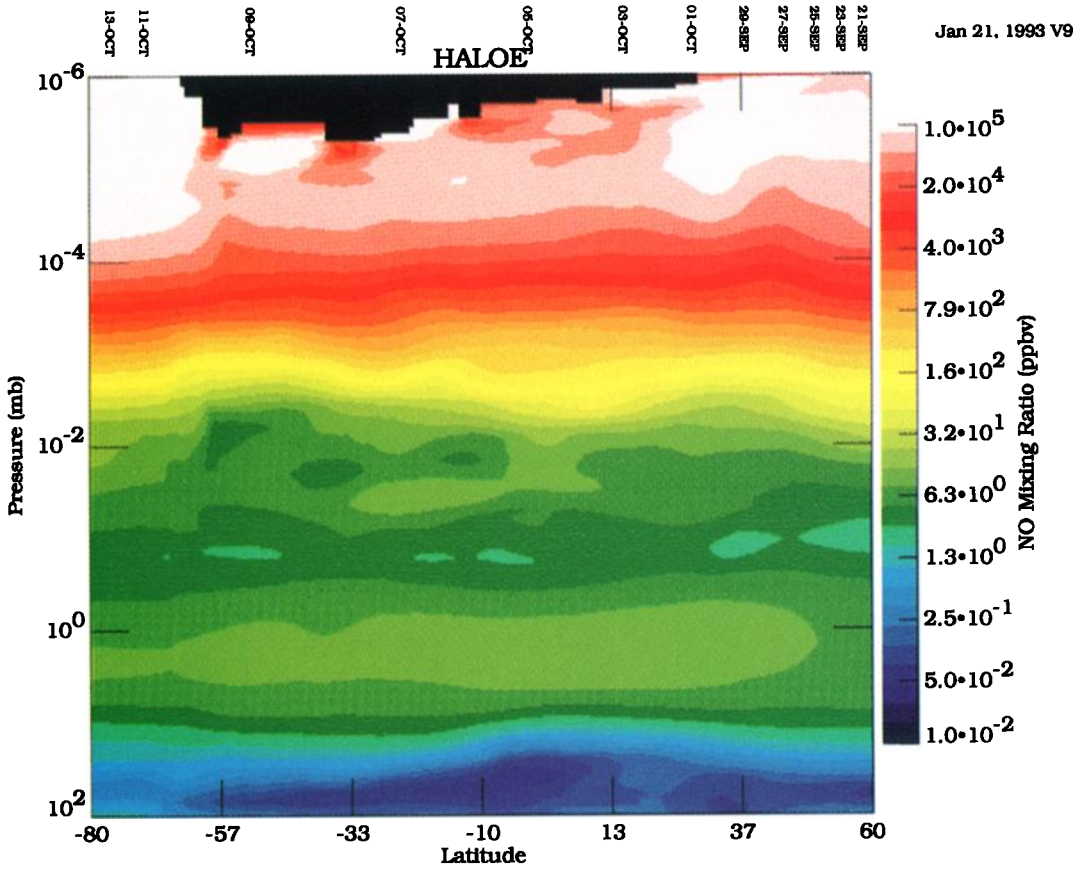

Plate 6. HALOE NO pressure versus latitude cross section, sunset for September 21 to October 15, 1992.

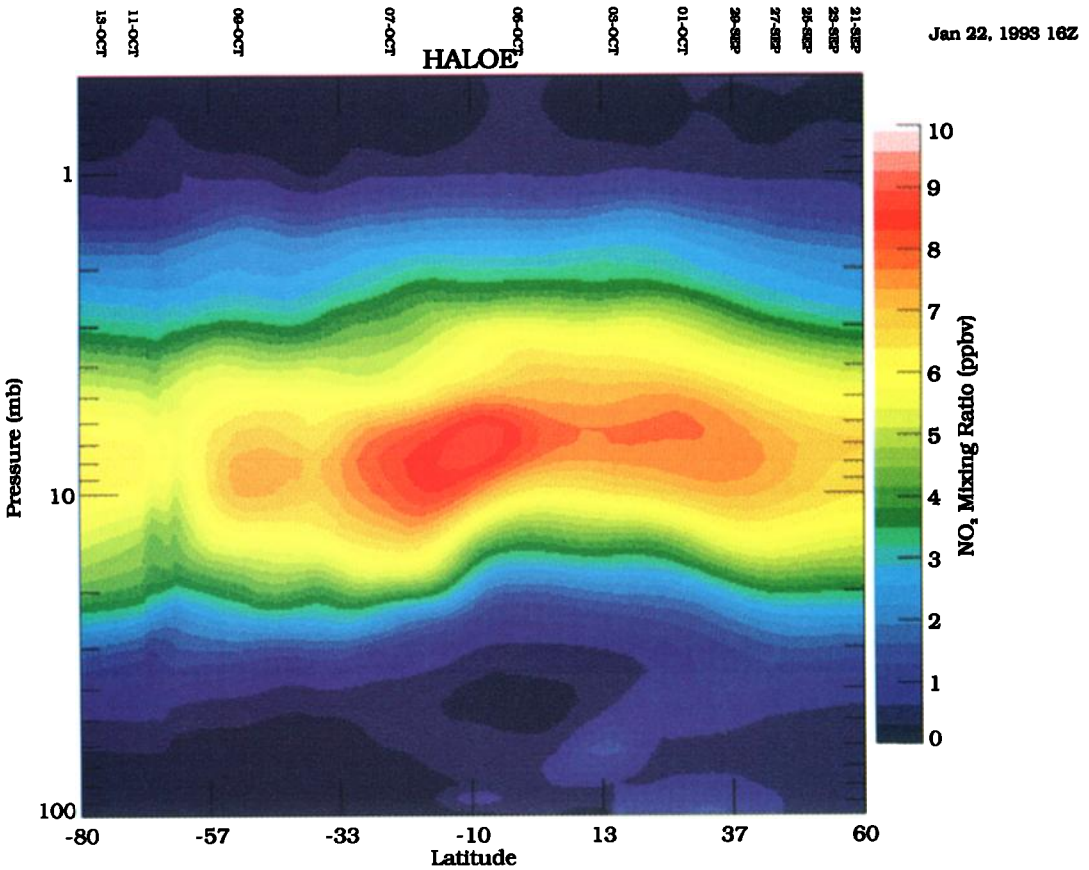

Plate 7. HALOE NO_2 pressure versus latitude cross section, sunset for September 21 to October 15, 1992.

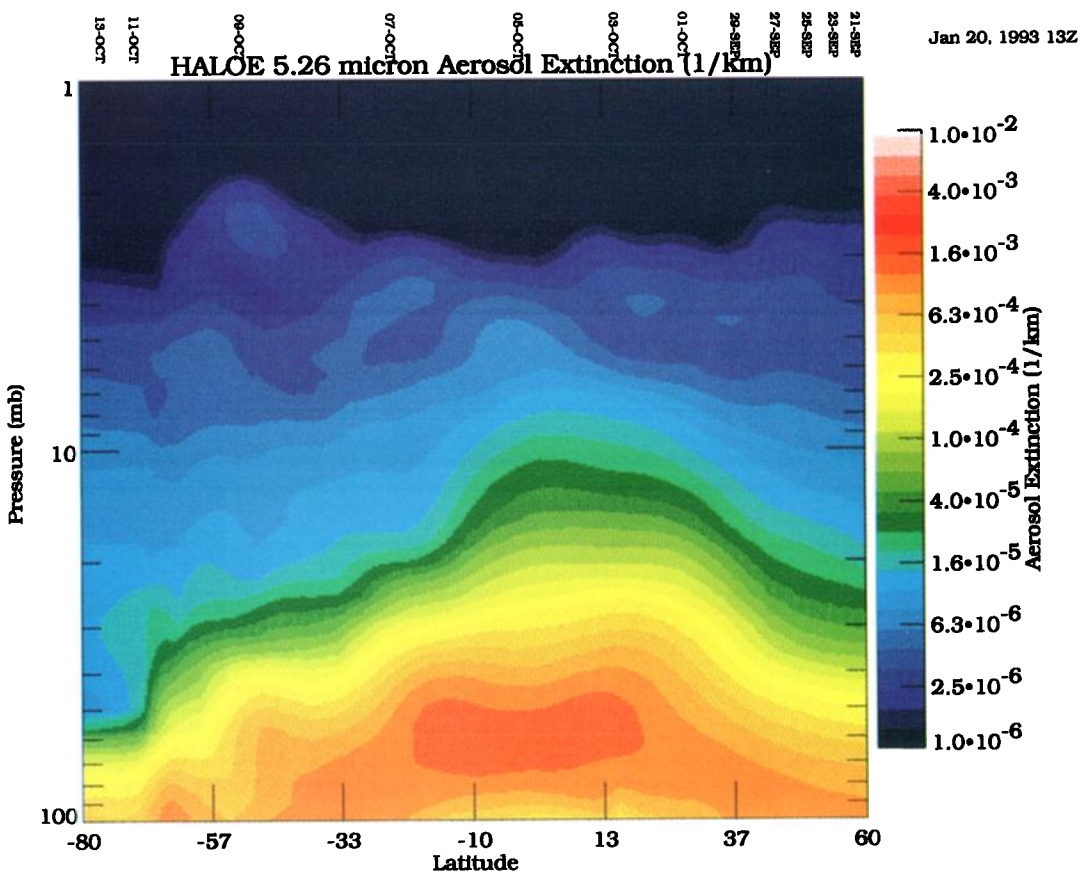

Plate 8. HALOE Aerosol extinction pressure versus latitude cross section, sunset for September 21 to October 15, 1992.

above the stratopause. The gradient at ≈ 65°S is most apparent in the NO_2 cross section, but it exists in the other cross sections as well and is associated with the boundary of the southern vortex. Studies are under way to assess the validity of this feature.

An aerosol extinction coefficient cross section obtained using the 5.26 μm NO channel is shown in Plate 8. This cross section shows enhanced aerosol extinction in the tropics and a downward slope of the contours toward both poles. Measurable aerosol extinction (> 2 x 10^{-6} km^{-1} for HALOE) is observed up to as high as the 2- or 3-mbar level in some latitude regions.

An example of a southern hemisphere global orthographic CH_4 projection on the 31.6-mbar pressure surface is shown in Plate 9. This plot covers the same time period as the latitude cross sections. The presence of low CH_4 is seen in the polar region inside the Antarctic vortex which, from independent wind and potential vorticity data, was mostly south of 60°S during this period. There were times when the vortex elongated and extended as far north as 45°S. It is clear that the low CH_4 characteristic of the vortex extends to at least 40°S. It is also evident that low CH_4 mixing ratio air from the vortex is affecting methane levels at 25°S. Trajectory studies are under way to determine how much of the low methane is due to vortex movement over the September 21 to October 15 time period as opposed to transport out of the vortex itself.

8. Summary

The HALOE experiment was successfully launched and activated on the UARS spacecraft. The orbital operation has been virtually flawless since science data collection began on October 11, 1991, up to the present January 30, 1992. Measurements are made continuously except for periods when solar grazing events occur, resulting in no occultations. The latitude coverage over a 1-year period ranges from 80°S to 80°N. Initial sunrise observations began in the Antarctic and sunsets occurred in the tropics. As of this writing, many measurement sweeps over broad latitude ranges have occurred providing coverage of all seasons in both hemispheres. All instrument performance criteria either meet or exceed specifications. The occurrence of the Mount Pinatubo aerosol layer has complicated HALOE orbital operations and has restricted the lower altitude range where useful measurements can be made to about 20 km in especially dense aerosol regions in the tropics. This lower limit has been achieved following considerable flight testing and unanticipated fine adjustments that were made to the pointer/tracker system using ground-issued commands.

The retrieved mixing ratios all look reasonable and extend to higher than expected altitudes. We particularly note that H_2O and O_3 extend to 80 km and 90 km respectively, and NO extends to 130 km. An extensive data validation program is under way, and initial comparisons with correlative underflight data are encouraging. Several internal consistency checks, including sunrise/sunset differences, HF versus CH_4 and H_2O versus CH_4 regressions, and comparison of pressure versus latitude cross-section features all give excellent results. Qualitative comparisons with 1985 Spacelab 3 ATMOS data show reasonable agreement. Therefore every indication from studies performed to date is that the data are of high quality and are suitable for application to scientific studies.

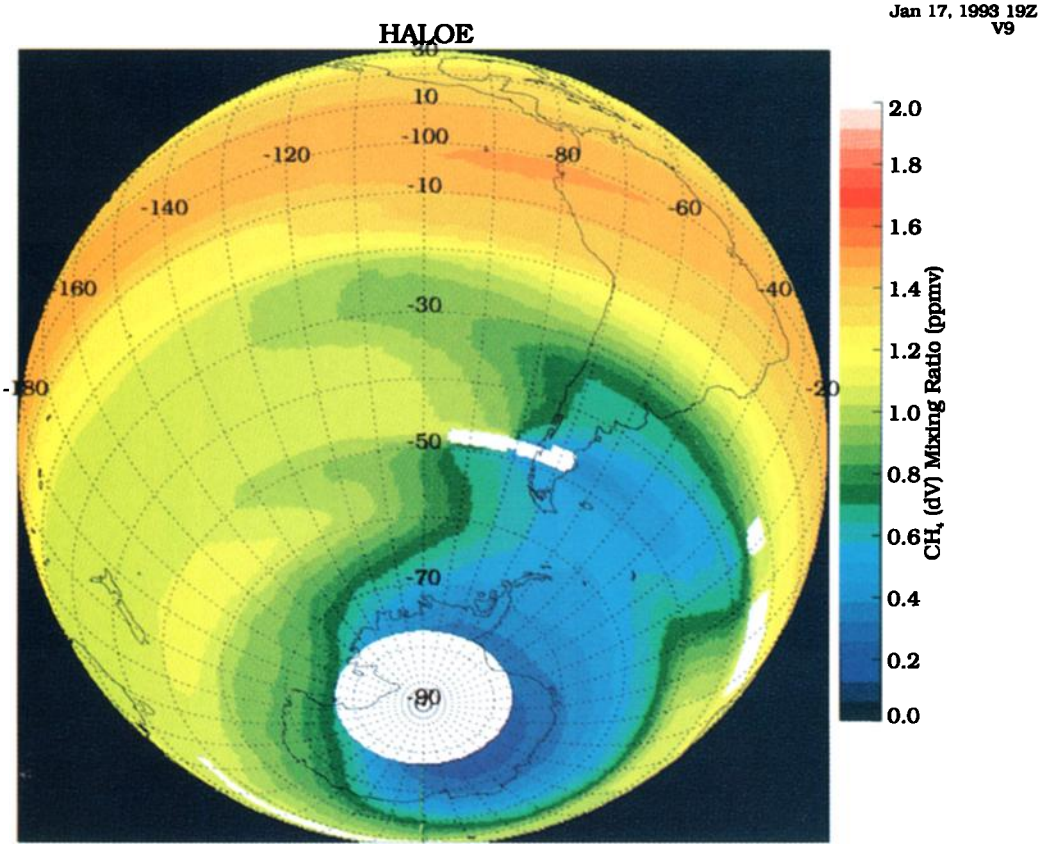

Plate 9. HALOE CH_4 31.6-mbar surface orthographic projection for September 21 to October 15, 1992.

Pressure versus latitude cross sections for the Antarctic spring time period show important features such as evidence of unmixed vertical descent in the south polar region, dehydration in the Antarctic lower stratosphere, the presence of a tropical hygropause, a continuous region of low H_2O from the Antarctic to the equator, effects of the Hadley tropical upwelling in the tracer molecules CH_4, HF, and H_2O, and the first global distributions of HCl, HF, and NO. A global orthographic plot for the same time period shows clear evidence that Antarctictype air exists as far north as 40°S, and the effects of this air are seen in the tropics at 25°S. Once the validation effort is complete, detailed scientific investigations will be carried out using these and other features of the data.

Acknowledgments. We acknowledge Sheila D. Johnson for her efforts in typing this manuscript, Martin G. Mlynczak for his timely assistance, and the many other engineers and scientists at both the Langley Research Center and TRW, Inc., who worked diligently to make the instrument perform properly. We especially acknowledge James L. Raper, Dewey M. Smith (deceased), and Thomas C. Jones who served as project managers during the HALOE development. We owe a debt of gratitude to each for their diligent service and commitment to excellence. We also thank Kenneth A. Stone for generating the latitude cross sections and the global orthographic plot.

References

Connor, B. J., and C. D. Rodgers, A comparison of retrieval methods: Optimal estimation, onion peeling, and a combination of the two, in *RSRM 1987: Advances in Remote Sensing Retrieval Methods*, edited by A. Deepak, H. E. Fleming, and J. S. Theon, Editors, A. Deepak, Hampton, 1989.

Farman, J. C., B. G. Gardiner, and J. D. Shanklin, Large losses of total ozone in Antarctica reveal seasonal ClO_x/NO_x interaction, *Nature*, *315*, 207-210, 1985.

Farmer, C. B., O. F. Raper, and F. G. O'Callaghan, Final report on the first flight of the ATMOS instrument during the Spacelab 3 mission, April 29 through May 6, 1985, *Jet Propul. Lab. Publ. 87-32*, 1987.

Hervig, M. E., J.M. Russell III, L.L. Gordley, J.H. Park, and S.R. Drayson, Observations of aerosol by the HALOE experiment onboard UARS: a preliminary validatuon, *Geophys. Res. Lett.*, In Press, 1993.

Harrison, E. F., and G. G. Gibson, Orbital analysis for the Upper Atmosphere Research Satellite missions, *J. Spacecr. Rockets*, *18*, March/April 1981.

Mankin, W. F., M. T. Coffey, and M. C. Abrams, Trends of column amounts of stratospheric trace gases determined from airborne infrared observations, paper presented at the IUGG Middle Atmosphere Science Symposium, Int. Union of Geol. Geophysics, Vienna, Austria, August 1991.

Molina, M. J., and F. S. Rowland, Stratospheric sink for chlorofluoromethanes: Chlorine atom catalyzed destruction of ozone, *Nature*, *249*,810-812, 1974.

Park, J. H., J. M. Russell, and S. R. Drayson, Pressure sensing of the atmosphere by solar occultation using broadband CO_2 absorption, *Appl. Opt.*, *18*, 1950-1954, 1979.

Reichle, H. G., V. S. Connors, J. A. Holland, R. T. Sherrill, H. A. Wallio, J. C. Casas, E. P. Condon, B. B. Gormsen, and W. Seiler, The distribution of middle tropospheric carbon monoxide during early 1984, *J. Geophys. Res.*, *95*, 9845-9856, 1990.

Rodgers, C. D., Characterization and error analysis of profiles retrieved from remote sounding measurements, *J. Geophys. Res.*, *95*, 5587-5595, 1990.

Russell, J. M., III, et al., HALOE Antarctic Observations in the Spring of 1991, *Geophys. Res. Lett., 20*, 719-722, 1993.

Russell, J. M., III, Satellite solar occultation sounding of the middle atmosphere, *Pure Appl. Geophys.*, *118*, 616-635, 1980.

Russell, J. M. III, J. H. Park, and S. R. Drayson, Global monitoring of stratospheric halogen compounds from a satellite using gas filter spectroscopy in the solar occultation mode, *Appl. Opt.*, *16*, No. 3, 607-612, March, 1977.

Solomon, S., Antarctic ozone: Progress towards a quantitative understanding of Antarctic ozone depletion, *Nature*, *347*, 347-354, 1990.

Tuck, A. F., James M. Russell III, and John E. Harries, Stratospheric Dryness: Antiphased Desiccation over Micronesia and Antarctica, *Geophys. Res. Lett.*, In press, 1993.

World Meteorological Organization (WMO), Scientific assessment of stratospheric ozone: 1989, WMO Global Ozone Research and Monitoring Project, *WMO Rep. 20*, Geneva, 1990.

R. J. Cicerone, University of California/Irvine, Irvine, CA 92717.

P. J. Crutzen, Max Planck Institute for Chemistry, Mainz, Germany.

S. R. Drayson, University of Michigan, Ann Arbor, MI 48105.

J. E. Frederick, University of Chicago, Chicago, IL 60637.

L. L. Gordley, GATS, Incorporated, Hampton, VA 23665.

J. E. Harries, Rutherford Appleton Laboratory, Oxfordshire, England.

W. D. Hesketh, SpaceTec Ventures, Incorporated, Hampton, VA 23665.

J. H. Park and J. M. Russell III, Atmospheric Sciences Division, Mail Stop 401B, NASA Langley Research Center, Hampton, VA 23681-0001.

A. F. Tuck, NOAA Aeronomy Laboratory, Boulder, CO 80303.

(Received February 28, 1992;
revised February 4, 1993;
accepted February 4, 1993.)